Molecular Pharmacology Fast Forward. Published on July 27, 2021 as DOI: 10.1124/molpharm.121.000270
This article has not been copyedited and formatted. The final version may differ from this version.

Acylation of the incretin peptide exendin-4 directly impacts GLP-1 receptor signalling and trafficking

Maria Lucey[1], Tanyel Ashik[1], Amaara Marzook[1], Yifan Wang[2], Joëlle Goulding[3,4], Atsuro Oishi[5,6], Johannes Broichhagen[7], David J Hodson[4,8,9], James Minnion[1], Yuval Elani[10], Ralf Jockers[5], Stephen J Briddon[3,4], Stephen R Bloom[1], Alejandra Tomas[2, #], Ben Jones[1, #].

[#] Co-senior authors

[1] Section of Endocrinology and Investigative Medicine, Department of Metabolism, Digestion and Reproduction, Imperial College London, London, W12 0NN, UK.

[2] Section of Cell Biology and Functional Genomics, Department of Metabolism, Digestion and Reproduction, Imperial College London, London, W12 0NN, UK.

[3] Division of Physiology, Pharmacology and Neuroscience, School of Life Sciences, University of Nottingham, Nottingham, NG7 2UH, UK.

[4] Centre of Membrane Proteins and Receptors (COMPARE), University of Birmingham and University of Nottingham, Midlands, UK.

[5] Université de Paris, Institut Cochin, INSERM, CNRS, F-75014 Paris, France.

[6] Department of Anatomy, Kyorin University Faculty of Medicine, Tokyo, Japan.

[7] Leibniz-Forschungsinstitut für Molekulare Pharmakologie, Robert-Rössle-Str. 10, 13125 Berlin, Germany.

[8] Institute of Metabolism and Systems Research (IMSR), University of Birmingham, Birmingham, UK.

[9] Centre for Endocrinology, Diabetes and Metabolism, Birmingham Health Partners, Birmingham, UK.

[10] Department of Chemical Engineering, Imperial College London, Exhibition Road, London, UK.

Downloaded from molpharm.aspetjournals.org at ASPET Journals on April 20, 2024

Molecular Pharmacology Fast Forward. Published on July 27, 2021 as DOI: 10.1124/molpharm.121.000270
This article has not been copyedited and formatted. The final version may differ from this version.

Running title: Pharmacology of acylated exendin-4

Corresponding authors:

Ben Jones, Section of Endocrinology and Investigative Medicine, Department of Metabolism, Digestion and Reproduction, Imperial College London, London, W12 0NN, United Kingdom.

Email: ben.jones@imperial.ac.uk; Telephone: 020 331 30348

Alejandra Tomas, Section of Cell Biology and Functional Genomics, Department of Metabolism, Digestion and Reproduction, Imperial College London, London, W12 0NN, United Kingdom.

Email: a.tomas-catala@imperial.ac.uk; Telephone: 020 7594 3364

Number of pages: 45

Number of tables: 1

Number of figures: 5

Number of references: 72

Word count (Abstract): 248

Word count (Introduction): 641

Word count (Discussion): 1611

Abbreviations

BRET	Bioluminescence resonance energy transfer
BSA	Bovine serum albumin
CyOFP	Cyan-excitable orange fluorescent protein
DERET	Diffusion-enhanced resonance energy transfer
FCS	Fluorescence correlation spectroscopy
FITC	Fluorescein isothiocyanate
GFP	Green fluorescent protein

Downloaded from molpharm.aspetjournals.org at ASPET Journals on April 20, 2024

Molecular Pharmacology Fast Forward. Published on July 27, 2021 as DOI: 10.1124/molpharm.121.000270
This article has not been copyedited and formatted. The final version may differ from this version.

GLP-1(R)(A)	Glucagon-like peptide-1 (receptor) (agonist)
GUV	Giant unilameller vesicle
MβCD	Methyl-β-cyclodextrin
Nb37	Nanobody-37
POPC	1-palmitoyl-2-oleoyl-sn-glycero-3-phosphocholine
T2D	Type 2 diabetes
TMR	Tetramethylrhodamine
TR-FRET	Time-resolved Förster resonance energy transfer

Downloaded from molpharm.aspetjournals.org at ASPET Journals on April 20, 2024

Molecular Pharmacology Fast Forward. Published on July 27, 2021 as DOI: 10.1124/molpharm.121.000270
This article has not been copyedited and formatted. The final version may differ from this version.

Abstract

The glucagon-like peptide-1 receptor (GLP-1R) is a class B G protein-coupled receptor and mainstay therapeutic target for the treatment of type 2 diabetes and obesity. Recent reports have highlighted how biased agonism at the GLP-1R affects sustained glucose-stimulated insulin secretion through avoidance of desensitisation and downregulation. A number of GLP-1R agonists (GLP-1RAs) feature a fatty acid moiety to prolong their pharmacokinetics via increased albumin binding, but the potential for these chemical changes to influence GLP-1R function has rarely been investigated beyond potency assessments for cyclic adenosine monophosphate (cAMP). Here we directly compare the prototypical GLP-1RA exendin-4 with its C-terminally acylated analogue, exendin-4-C16. We examine relative propensities of each ligand to recruit and activate G proteins and β-arrestins, endocytic and post-endocytic trafficking profiles, and interactions with model and cellular membranes in HEK293 and HEK293T cells. Both ligands had similar cAMP potency but exendin-4-C16 showed ~2.5-fold bias towards G protein recruitment and a ~60% reduction in β-arrestin-2 recruitment efficacy compared to exendin-4, as well as reduced GLP-1R endocytosis and preferential targeting towards recycling pathways. These effects were associated with reduced movement of the GLP-1R extracellular domain measured using a conformational biosensor approach, and a ~70% increase in insulin secretion in INS-1 832/3 cells. Interactions with plasma membrane lipids were enhanced by the acyl chain. Exendin-4-C16 showed extensive albumin binding and was highly effective for lowering of blood glucose in mice over at least 72 hours. Our study highlights the importance of a broad approach to the evaluation of GLP-1RA pharmacology.

Significance statement

Acylation is a common strategy to enhance the pharmacokinetics of peptide-based drugs. Our work shows how acylation can also affect various other pharmacological parameters, including biased agonism, receptor trafficking and interactions with the plasma membrane, which may be therapeutically important.

Downloaded from molpharm.aspetjournals.org at ASPET Journals on April 20, 2024

Molecular Pharmacology Fast Forward. Published on July 27, 2021 as DOI: 10.1124/molpharm.121.000270
This article has not been copyedited and formatted. The final version may differ from this version.

Downloaded from molpharm.aspetjournals.org at ASPET Journals on April 20, 2024

Molecular Pharmacology Fast Forward. Published on July 27, 2021 as DOI: 10.1124/molpharm.121.000270
This article has not been copyedited and formatted. The final version may differ from this version.

1 Introduction

Type 2 diabetes (T2D) affects over 400 million people worldwide and leads to chronic illnesses including blindness, nerve damage, kidney failure and cardiac disease (Guariguata *et al.*, 2014). Pathological increases in blood glucose, the central metabolic defect in T2D, occur chiefly due to failure of pancreatic beta cells to release enough of the glucoregulatory hormone insulin, and overweight-related tissue resistance to insulin action. Therefore, pharmacological targeting of the glucagon-like peptide-1 receptor (GLP-1R), a class B G protein-coupled receptor (GPCR) which increases insulin release in a glucose-dependent manner and also suppresses appetite leading to weight loss, is an effective strategy against T2D (Graaf *et al.*, 2016). As GLP-1(7-36)NH_2, the endogenous ligand for GLP-1R, is enzymatically inactivated in the circulation within minutes and eliminated by glomerular filtration, a number of strategies have been used to develop pharmaceutically viable peptide GLP-1R agonists (GLP-1RAs) which remain active in the circulation for hours or days (A Andersen *et al.*, 2018). As typified by exendin-4 (in clinical use as exenatide), the peptide amino acid sequence can be altered to prevent proteolytic degradation, extending circulatory half-life from minutes to hours, whilst retaining full activity at the receptor (Kolterman *et al.*, 2003). An alternative or complementary approach, the best known exemplars of which are liraglutide and semaglutide (Lau *et al.*, 2015), involves attachment of a fatty acid side chain to the peptide to allow it to bind reversibly to albumin. Specifically, liraglutide includes a palmitic (C16) acid chain, which was switched to a C18 fatty diacid chain in semaglutide to improve affinity for human albumin (Knudsen and Lau, 2019). As albumin exceeds the size limit for glomerular filtration, this major elimination route is lost (Malm-Erjefält *et al.*, 2010). Half-life protraction of semaglutide via this strategy allows once-weekly administration in humans (Knudsen and Lau, 2019).

Whilst GLP-1RA pharmacology has been traditionally assessed by measuring cyclic adenosine monophosphate (cAMP) responses, additional factors are now recognised as important determinants of insulin release. For example, changes to the amino acid sequence of GLP-1R peptide agonists in their receptor core-facing N-terminal region can lead to bias

Downloaded from molpharm.aspetjournals.org at ASPET Journals on April 20, 2024

Molecular Pharmacology Fast Forward. Published on July 27, 2021 as DOI: 10.1124/molpharm.121.000270
This article has not been copyedited and formatted. The final version may differ from this version.

between G protein signalling, β-arrestin recruitment and receptor endocytosis (H Zhang *et al.*, 2015; Jones *et al.*, 2018). We recently reported how a dual strategy based on both pharmacokinetically preferential acylation and G protein-directed biased agonism could optimise GLP-1R therapeutic efficacy (Lucey *et al.*, 2020). Whilst not explored in detail in the latter project, we observed that the addition of a C-terminal acyl chain further influenced the ability of each ligand to recruit G proteins and β-arrestins to the GLP-1R, highlighting this feature as a modifier of GLP-1R efficacy in its own right.

Moreover, it is conceivable that acylation could constructively influence the interaction between agonist and plasma membrane by conferring distinct physicochemical properties, as suggested for the acylated analogues of glucagon-like peptide-2 (GLP-2) (Trier *et al.*, 2014). This has the potential to modulate downstream signalling by directing the ligand towards GLP-1Rs situated in sub-microscopic membrane domains variably enriched with signalling effectors on the cytoplasmic side (Villar *et al.*, 2016). Indeed, differences in segregation of activated GLP-1Rs into these “membrane rafts” are an important feature of biased agonist action (Buenaventura *et al.*, 2019).

To investigate these possibilities, in this study we performed a detailed comparison of the prototypical GLP-1R therapeutic agonist exendin-4 with an equivalent peptide bearing a C16 fatty diacid at its C-terminus, focusing on the relative propensities of each ligand to engage with G protein and β-arrestin recruitment and activation, endocytosis and post-endocytic sorting in HEK293 and HEK293T cells. We also evaluated interactions made by each ligand with giant unilamellar vesicles (GUVs) and the relative impact of modulating cellular cholesterol levels on GLP-1R signalling with each ligand. Our study highlights how installation of an acyl chain at the C-terminus influences multiple pharmacological properties of exendin-4, enhancing its ability to stimulate insulin release from pancreatic beta cells.

Downloaded from molpharm.aspetjournals.org at ASPET Journals on April 20, 2024

Molecular Pharmacology Fast Forward. Published on July 27, 2021 as DOI: 10.1124/molpharm.121.000270
This article has not been copyedited and formatted. The final version may differ from this version.

2 Materials and methods

2.1 Peptides and reagents

All peptides were obtained Wuxi Apptec (Wuhan, China) and were at least 90% pure. Laboratory reagents were obtained from Sigma Aldrich (Dorset, UK) unless otherwise specified.

2.2 Cell culture

HEK293T cells were maintained in DMEM supplemented with 10% FBS and 1% penicillin/streptomycin. HEK293-SNAP-GLP-1R cells generated by stable transfection of pSNAP-GLP-1R (Cisbio, Paris, France) into HEK293 cells (Buenaventura *et al.*, 2019) were used for some experiments, and maintained in DMEM supplemented with 10% FBS, 1% penicillin/streptomycin and 1 mg/ml G418. T-REx-SNAP-GLP-1R cells (Fang, Chen, Manchanda, *et al.*, 2020), generated from parental Flp-In™ T-REx™ 293 cells (Thermo Fisher Scientific, MA, USA) by Flp-mediated genomic integration of an insert encoding human GLP-1R with an N-terminal $SNAP_f$-tag and C-terminal SmBiT tag (custom synthesised by Genewiz, Steiβlingen, Germany), with pcDNA5/FRT as the backbone, were maintained in DMEM supplemented with 10% FBS and 1% penicillin/streptomycin. SNAP-GLP-1R expression was induced using 0.1 µg/ml tetracycline for 24 hours prior to experiments. PathHunter GLP-1R β-arrestin-1 and -2 cells (DiscoverX) were maintained in Ham's F12 medium with 10% FBS and 1% penicillin/streptomycin. INS-1 832/3 cells (a gift from Prof Christopher Newgard, Duke University) (Hohmeier *et al.*, 2000) were maintained in RPMI at 11 mM glucose, supplemented with 10% FBS, 10 mM HEPES, 1 mM pyruvate, 1 mM pyruvate, 50 µM β-mercaptoethanol and 1% penicillin/streptomycin.

Downloaded from molpharm.aspetjournals.org at ASPET Journals on April 20, 2024

Molecular Pharmacology Fast Forward. Published on July 27, 2021 as DOI: 10.1124/molpharm.121.000270
This article has not been copyedited and formatted. The final version may differ from this version.

2.3 Equilibrium GLP-1R binding assays

HEK293-SNAP-GLP-1R cells were labelled using 40 nM SNAP-Lumi4-Tb (Cisbio) in complete medium for 60 min at room temperature. After washing, cells were resuspended in HBSS containing 0.1% BSA and metabolic inhibitors (10 mM NaN_3 and 20 mM 2-deoxyglucose) to prevent endocytosis (Widmann *et al.*, 1995). After 20 min at room temperature, cells in 96-well white plates were equilibrated to 4°C before addition of agonists. To measure binding parameters for exendin-4 and exendin-4-C16, these non-labelled ligands were added alongside 10 nM exendin(9-39)-FITC and incubated for 24 hours in the dark to allow binding equilibrium to be achieved. TR-FRET signal from each well was then recorded using a Flexstation 3 with the following settings: λ_{ex} 340 nm, λ_{em} 520 and 620 nm, auto-cutoff, delay 50 µs, integration time 300 µs. A saturation binding isotherm for exendin(9-39)-FITC was performed during each experiment, and the K_i values for competing agonists were determined using the "Fit K_i" preset of Prism 8.0. To measure saturation binding for FITC- or TMR-labelled exendin-4 and exendin-4-C16 directly, these ligands were added to cells and incubated as above, followed by measurement of TR-FRET signal using the following settings: FITC ligands: λ_{ex} 340 nm, λ_{em} 520 and 620 nm, auto-cutoff, delay 50 µs, integration time 300 µs; TMR ligands: λ_{ex} 340 nm, λ_{em} 550 and 610 nm, auto-cutoff, delay 50 µs, integration time 300 µs.

2.4 Measurement of cAMP production

HEK293-SNAP-GLP-1R cells were resuspended in serum-free medium and treated at 37°C with indicated concentration of agonist for 30 min. cAMP was then assayed by HTRF (Cisbio cAMP Dynamic 2) using a Spectramax i3x plate reader (Molecular Devices). Where indicated, cells were pre-incubated with methyl-β-cyclodextrin in advance of the assay before washing.

Downloaded from molpharm.aspetjournals.org at ASPET Journals on April 20, 2024

Molecular Pharmacology Fast Forward. Published on July 27, 2021 as DOI: 10.1124/molpharm.121.000270
This article has not been copyedited and formatted. The final version may differ from this version.

2.5 NanoBiT assay

The assay was performed as previously described (Lucey *et al.*, 2020). HEK293T cells in 12-well plates were transfected with 0.5 µg GLP-1R-SmBiT plus 0.5 µg LgBiT-mini-G_s (Wan *et al.*, 2018) (a gift from Prof Nevin Lambert, Medical College of Georgia, USA), or with 0.05 µg GLP-1R-SmBiT and 0.05 µg LgBit-β-arrestin-2 (Promega, Hampshire, UK) plus 0.9 µg pcDNA3.1 for 24 hours. Cells were detached with EDTA, resuspended in HBSS, and furimazine (Promega) was added at a 1:50 dilution from the manufacturer's pre-prepared stock. After dispensing into 96-well white plates, a baseline read of luminescent signal was serially recorded over 5 min using a Flexstation 3 instrument (Molecular Devices) at 37°C before addition of the indicated concentration of ligand, after which signal was repeatedly recorded for 30 min. Results were expressed relative to individual well baseline and AUC was calculated. Each assay was performed with both pathways measured in parallel using the same ligand stocks. Bias between mini-G_s and β-arrestin-2 recruitment was determined similarly to earlier work (Pickford *et al.*, 2020), by subtracting the $\log\tau/K_A$ values (Kenakin *et al.*, 2012) for each ligand in each pathway for each assay to determine $\Delta \log\tau/K_A$ (referred to here as Δ LogR); this indicates the relative pathway preference for each ligand which can then be compared statistically.

2.6 β-arrestin-1 and -2 recruitment by enzyme complementation

PathHunter GLP-1R β-arrestin-1 or -2 cells were treated in serum-free medium for 30 min with a range of agonist concentrations before addition of PathHunter chemiluminescent detection reagents. Bias was assessed as in Section 2.5.

2.7 β-arrestin conformational change assay

The assay was adapted from a previous description (Oishi *et al.*, 2019). HEK293T cells were seeded in 6-well plates and transfected with 0.5 µg NLuc-β-arrestin-2-CyOFP under a TK promoter, 0.5 µg SNAP-GLP-1R under a CMV promoter, plus 1 µg pcDNA3.1, for 24 hours

Downloaded from molpharm.aspetjournals.org at ASPET Journals on April 20, 2024

Molecular Pharmacology Fast Forward. Published on July 27, 2021 as DOI: 10.1124/molpharm.121.000270
This article has not been copyedited and formatted. The final version may differ from this version.

before the assay. Alternatively, stable HEK293-SNAP-GLP-1R cells in 6-well plates were transfected with 0.5 µg NLuc-β-arrestin-2-CyOFP plus 1.5 µg pcDNA3.1. Cells were detached with EDTA, resuspended in HBSS with furimazine (1:50 dilution). After dispensing into 96-well white plates, a baseline read of luminescent signals at both 460 nm and 575 nm was serially recorded over 5 min using a Flexstation 3 instrument at 37°C. Ligands in HBSS were then added, after which signal was repeatedly recorded for 30 min. Results were first normalised to individual well baseline and then to the average vehicle signal within each assay (see Supplementary Figure 5A). Statistical comparisons were performed on AUC calculated from each ligand-induced kinetic trace.

2.8 G protein activation assay by Nb37 BRET

A construct encoding SNAP-GLP-1R with a C-terminal nanoluciferase was generated in house by PCR cloning of the nanoLuciferase sequence from pcDNA3.1-ccdB-Nanoluc (a gift from Mikko Taipale; Addgene plasmid # 87067) onto the C-terminus end of the SNAP-GLP-1R vector (Cisbio), followed by site-directed mutagenesis of the GLP-1R stop codon. HEK293T cells in 6-well plates were transfected with 0.2 µg SNAP-GLP-1R-NLuc, 0.2 µg Nb37-GFP (a gift from Dr Roshanak Irranejad, UCSF), plus 1.6 µg pcDNA3.1, for 24 hours before the assay. Cells were detached with EDTA, resuspended in HBSS, and furimazine was added at a 1:50 dilution from the manufacturer's pre-prepared stock. After dispensing into 96-well white plates, a baseline read of luminescent signals at both 460 nm and 525 nm was serially recorded over 5 min using a Flexstation 3 instrument at 37°C. Ligands in HBSS were then added, after which signal was repeatedly recorded for 30 min. Results were first normalised to individual well baseline and then to the average vehicle signal from each assay (see Supplementary Figure 5B). Statistical comparisons were performed on AUC calculated from each ligand-induced kinetic trace.

Downloaded from molpharm.aspetjournals.org at ASPET Journals on April 20, 2024

Molecular Pharmacology Fast Forward. Published on July 27, 2021 as DOI: 10.1124/molpharm.121.000270
This article has not been copyedited and formatted. The final version may differ from this version.

2.9 Preparation and imaging of fixed cell samples

Cells were seeded onto coverslips coated with 0.1% poly-D-lysine and allowed to adhere overnight. Where relevant, transfection was performed as for functional assays and surface labelling of SNAP-tagged GLP-1R was performed using 0.5 µM of the indicated SNAP-Surface probe for 30 min at 37°C before washing with HBSS. Ligands were applied in Ham's F12 media containing 0.1% BSA at 37°C. For fixation, 4% paraformaldehyde (PFA) was applied directly to the medium for 15 min before washing with PBS. Slides were mounted in Prolong Diamond antifade with DAPI (Thermo Fisher Scientific, MA, USA) and allowed to set overnight. Imaging was performed using a Nikon Ti2E custom microscope platform with automated stage (ASI) and LED light source controlled by µManager. High resolution z-stacks were acquired via a 100X 1.45 NA oil immersion objective, and used for image deconvolution using DeconvolutionLab2 (Sage *et al.*, 2017) with the Richardson-Lucy algorithm.

2.10 Measurement of GLP-1R internalisation by time-lapse high content microscopy

HEK293-SNAP-GLP-1R cells were seeded overnight in black, clear-bottom 96-well imaging plates coated with 0.1% poly-D-lysine. Cells were labelled with SNAP-Surface-649 (0.5 µM, from New England Biolabs, Hitchin, UK) for 30 min at 37°C. After washing, imaging medium was added to the wells (phenol red-free DMEM with 10 mM HEPES and 0.1% BSA) at 37°C. Baseline epifluorescence and transmitted phase contrast images were acquired using a 20X magnification 0.75 NA objective from 4 positions per well using the imaging system in Section 2.8. Further baseline epifluorescence images were acquired using a 40X magnification 0.95 NA objective, after which ligands were added directly to each well. Images in the same 4 positions were acquired every 3 min for 30 min. To quantify the translocation of surface-labelled SNAP-GLP-1R from plasma membrane to endosomes, a "spot-counting" imaging processing pipeline implemented in Fiji was developed as follows: 1) flatfield correction was applied to the epifluorescence images using BaSiC (Peng *et al.*, 2017); 2) Laplacian filtering (smoothening scale: 2.0) was applied using FeatureJ; 3) starting

Downloaded from molpharm.aspetjournals.org at ASPET Journals on April 20, 2024

Molecular Pharmacology Fast Forward. Published on July 27, 2021 as DOI: 10.1124/molpharm.121.000270
This article has not been copyedited and formatted. The final version may differ from this version.

with an image in which multiple endosomal puncta were visible, images were thresholded using the auto-selected threshold from the "Triangle" algorithm, and the same threshold was used for all images; 4) spots were counted using the particle counting algorithm in Fiji with a size limit of 0.5-5 µm, and roundness of 0.5-1; 5) differences in cell density within each image were accounted for by estimating confluence from the phase contrast image (cropped to the region covered by the 40X objective) using PHANTAST (Jaccard *et al.*, 2014) and dividing the spot count by this value; 6) after normalisation, the number of spots present at baseline was subtracted to identify the ligand-induced changes. Rate constants were determined from one-phase exponential curve fitting in Prism 8.0.

2.11 Measurement of GLP-1R internalisation by DERET

The assay was performed as previously described (Lucey *et al.*, 2020). HEK-SNAP-GLP-1R cells were labelled using 40 nM SNAP-Lumi4-Tb in complete medium for 60 min at room temperature. After washing, cells were resuspended in HBSS containing 24 µM fluorescein and dispensed into 96-well white plates. A baseline read was serially recorded over 5 min using a Flexstation 3 instrument at 37°C in TR-FRET mode with the following settings: λ_{ex} 340 nm, λ_{em} 520 and 620 nm, auto-cutoff, delay 400 µs, integration time 1500 µs. Ligands were then added, after which signal was repeatedly recorded for 30 min. Fluorescence signals were expressed ratiometrically after first subtracting signal from wells containing 24 µM fluorescein without cells. Internalisation was quantified as AUC relative to individual well baseline.

2.12 Measurement of GLP-1R trafficking to acidic endosomes using LysoTracker

HEK-SNAP-GLP-1R cells were labelled with SNAP-Lumi4-Tb (40 nM, 60 min at 37°C, in complete medium), with LysoTracker Red DND99 (100 nM) added for the last 15 min of the incubation period. After washing, labelled cells were resuspended in HBSS. TR-FRET signals at baseline and serially after agonist addition were recorded at 37°C using a

Downloaded from molpharm.aspetjournals.org at ASPET Journals on April 20, 2024

Molecular Pharmacology Fast Forward. Published on July 27, 2021 as DOI: 10.1124/molpharm.121.000270
This article has not been copyedited and formatted. The final version may differ from this version.

Flexstation 3 plate reader using the following settings: λ_{ex} = 335 nm, λ_{em} = 550 and 610 nm, delay 50 µs, integration time 300 µs. Receptor translocation to acidic endosomes was quantified as the ratio of fluorescent signal at 610 nm to that at 550 nm.

2.13 Measurement of receptor recycling by TR-FRET

The assay was performed as previously described (Fang, Chen, Pickford, *et al.*, 2020). Adherent HEK293-SNAP-GLP-1R cells in 96-well white plates coated with 0.1% poly-D-lysine were labelled with 40 nM BG-S-S-Lumi4-Tb in complete medium for 60 min at room temperature. After washing, cells were treated for 30 min with each agonist at 100 nM or vehicle (serum-free medium) to induce GLP-1R internalisation. Cells were then washed once with HBSS before application of alkaline TNE buffer (pH 8.6) containing (or not) 100 mM Mesna for 5 min at 4°C to cleave residual surface GLP-1R. 10 nM Luxendin645 (Ast *et al.*, 2020) in HBSS containing 0.1% BSA was then added and TR-FRET signal was serially monitored using a Spectramax i3x multi-mode plate reader with HTRF module. Ratiometric HTRF responses were normalised to baseline from the first 3 reads.

2.14 Measurement of GLP-1R compartmentalization by BRET

HEK293T cells in 6-well plates were transfected with 0.2 µg SNAP-GLP-1R-NLuc, 0.2 µg of KRAS-Venus, Rab5-Venus, Rab7-Venus or Rab11-Venus (kindly provided by Prof Nevin Lambert, Medical College of Georgia, and Prof Kevin Pfleger, University of Western Australia), plus 1.6 µg pcDNA3.1, 24 hours before the assay. Cells were detached with EDTA, resuspended in HBSS, and furimazine was added at a 1:50 dilution from the manufacturer's pre-prepared stock. After dispensing into 96-well white plates, a baseline read of luminescent signals at both 460 nm and 535 nm was serially recorded over 5 min using a Flexstation 3 instrument at 37°C. Ligands in HBSS were then added, after which signal was repeatedly recorded for 30 min. Results were first normalised to individual well baseline and then to the average vehicle signal from each experiment (see Supplementary

Downloaded from molpharm.aspetjournals.org at ASPET Journals on April 20, 2024

Molecular Pharmacology Fast Forward. Published on July 27, 2021 as DOI: 10.1124/molpharm.121.000270
This article has not been copyedited and formatted. The final version may differ from this version.

Figures 5C – 5F). Statistical comparisons were performed on AUC calculated from each ligand-induced kinetic trace.

2.15 Mini-G_s subcellular translocation assay

HEK293-SNAP-GLP-1R cells were seeded in 6-well plates and transfected with 0.2 µg plasmid DNA encoding mini-G_s-NLuc (a gift from Prof Nevin Lambert, Medical College of Georgia) (Wan *et al.*, 2018), 0.2 µg KRAS-Venus or Rab5-Venus, plus 1.6 µg pcDNA3.1, for 24 hours before the assay. Cells were detached with EDTA and resuspended in HBSS with furimazine (1:50 dilution). After dispensing into 96-well white plates, a baseline read of luminescent signals at both 460 nm and 535 nm was serially recorded over 5 min using a Flexstation 3 instrument at 37°C. Ligands in HBSS were then added, after which signal was repeatedly recorded for 30 min. Results were first normalised to individual well baseline and then to the average vehicle signal from each experiment (Supplementary Figures 5G and 5H). Statistical comparisons were performed on AUC calculated from each ligand-induced kinetic trace.

2.16 Insulin secretion assay

INS-1 832/3 cells were pre-incubated in complete medium at 3 mM glucose for 16 hours prior to the assay. After washing, cells were dispensed into 96-well plates containing 11 mM glucose ± the indicated concentration of agonist and incubated for 1 hour (acute secretion assay) or 16-18 hours (sustained secretion assay). Secreted insulin was analysed from a sample of diluted supernatant by immunoassay (Cisbio wide range HTRF assay, measured using a Spectramax i3x plate reader). Results were normalised to the glucose-only response.

Downloaded from molpharm.aspetjournals.org at ASPET Journals on April 20, 2024

Molecular Pharmacology Fast Forward. Published on July 27, 2021 as DOI: 10.1124/molpharm.121.000270
This article has not been copyedited and formatted. The final version may differ from this version.

2.17 Isolation and imaging of giant unilamellar vesicles

GUVs in the fluid phase, composed of 1-palmitoyl-2-oleoyl-sn-glycero-3-phosphocholine (POPC) lipid were prepared via electroformation. Lipids were purchased from Avanti Polar Lipids (AL, USA). First, lipid in chloroform (20 µl; 1 mg/mL) was spread evenly on a conductive indium tin oxide coated (ITO) slide, leaving a film which was dried under vacuum for 30 min to remove residual solvent. A 5 mm thick polydimethylsiloxane (PDMS) spacer with a central cut-out was used to separate the slides with the conductive sides facing each other, and the chamber was filled with a solution of 100 mM sucrose in DI water. An alternating electric field (1 V, 10 Hz) was applied across the ITO plates using a function generator (Aim-TTi, TG315). After 2 h, the electric field was changed to 1 V, 2 Hz for a further hour, and the resulting vesicles collected. Either acylated or non-acylated compounds were added to make a final concentration of 100 nmol/l, and the solution incubated for 30 min. For imaging, 10 ul of the vesicle suspension was added to 90 ul of 100 mM glucose in DI water in an imaging chamber, and the vesicles sedimented on the bottom of the glass slide. Confocal imaging was done on a Leica TCS SP5 confocal fluorescent microscope, with a 20X objective set with an 84.5 µm pinhole (1 airy unit). Samples were acquired at a frequency of 400 Hz with eight line averages. The excitation was achieved a wavelength of 495 nm with emission set at between 510 and 530 nm. The images were acquired in the midplane of the GUVs. During data collection, focal planes slightly above and below were viewed to confirm image acquisition from the midplane.

2.18 Peptide-membrane interaction assay by FRET

T-REx-SNAP-GLP-1R cells were pre-treated ± 0.1 µg/ml tetracycline to induce SNAP-GLP-1R expression. Cells were detached using EDTA, centrifuged, and the pellet washed before the assay. Cellular labelling was then performed for 5 min using freshly prepared NR12S (Kucherak *et al.*, 2010), a gift from Prof Andrey Klymchenko, University of Strasbourg, at the indicated concentration in PBS in the dark. After washing three times to remove unbound probe, cells were dispensed into black 96-well microplates containing FITC-conjugated

Downloaded from molpharm.aspetjournals.org at ASPET Journals on April 20, 2024

Molecular Pharmacology Fast Forward. Published on July 27, 2021 as DOI: 10.1124/molpharm.121.000270
This article has not been copyedited and formatted. The final version may differ from this version.

peptides at a final concentration of 100 nM. FRET measurements were taken using a Flexstation 3 instrument with the following settings: λ_{ex} 475 nm, λ_{em} range 520 – 680 nm in 5 nm increments, cutoff 495 nm. Recorded fluorescence intensities were then normalised to 525 nm to allow for well-to-well differences and signal quenching by FRET. The normalised spectral trace from wells containing cells without NR12S probe was subtracted to determine probe-related FRET signal, which was quantified as AUC between 525 and 680 nm. Gaussian fitting was performed to determine the peak emission wavelength and relative intensity.

2.19 GLP-1R conformational sensor assay

HEK293-SNAP-GLP-1R cells were labelled with Lumi4-Tb (40 nM, 60 min at 37°C, in complete medium). After washing, cells were resuspended in HBSS containing NR12S (50 nM) and seeded into half-area opaque white plates. Baseline signal was measured for 5 min at 37°C using a Flexstation 3 plate reader with the following settings: λ_{ex} = 335 nm, λ_{em} = 490 and 590 nm, delay 50 µs, integration time 300 µs. Ligands were then added, and signal was serially monitored for 10 min. The TR-FRET ratio, i.e. the ratio of fluorescence intensities at 590 and 490 nm, was considered indicative of the proximity of the GLP-1R extracellular domain (ECD) to the plasma membrane.

2.20 Assessment of cAMP signalling from membrane nanodomains by FRET

T-REx-SNAP-GLP-1R cells were transfected for 36 hours with 2 µg per well of 6 well plate of the cAMP biosensor AKAP79-CUTie (a gift from Prof Manuela Zaccolo, University of Oxford) (Surdo *et al.*, 2017). 6 hours after transfection cells were transferred to black, clear bottom imaging microplates in complete medium containing 0.1 µg/ml tetracycline to induce SNAP-GLP-1R expression over 24 hours. For imaging experiments, adherent cells in HBSS underwent FRET imaging by widefield microscopy using an image splitter (Cairn Optosplit III) to separate CFP- and YFP-wavelength emission light into separate images on the

Downloaded from molpharm.aspetjournals.org at ASPET Journals on April 20, 2024

Molecular Pharmacology Fast Forward. Published on July 27, 2021 as DOI: 10.1124/molpharm.121.000270
This article has not been copyedited and formatted. The final version may differ from this version.

camera chip. Images were acquired every second for a 1 min baseline period and then for 5 min after addition of a saturating 1 µM agonist concentration. Channel registration was performed using the Cairn Image Splitter plugin for ImageJ. Phase contrast images were used for segmentation, allowing quantification of mean fluorescence intensity from cell-containing and background fluorescence, with the latter being subtracted before calculation of cell-associated FRET ratio from each image. FRET signal was normalised to t=0 and then to the vehicle response. For plate reader experiments, FRET signal was monitored from wells before and up to 12 min after addition of a range of concentrations of each agonist using a Flexstation 3 plate reader at 37°C and the following settings: λ_{ex} = 440 nm, λ_{em} = 485 and 535 nm. FRET was quantified as the ratio of fluorescent signal at 535 nm to that at 485 nm after subtraction of background signal at each wavelength. Cisbio lysis buffer was added immediately after completing the read and total cAMP was determined by HTRF. Concentration response curves were determined from average FRET signal from 8-12 min as well as the HTRF cAMP results to allow comparison of responses at an equivalent time-point.

2.21 Fluorescence correlation spectroscopy (FCS)

FCS was performed as previously described (Corriden *et al.*, 2014) on a Zeiss LSM 510NLO ConfoCor 3 microscope fitted with a 40X c-Apochromat 1.2 NA water-immersion objective. 30 s reads were taken at 22°C with a Diode-pumped solid-state (DPSS) 561nm laser excitation at ~0.2 $kWcm^{-2}$, emission collected through a 580-610nm bandpass and the pinhole set to 1 airy unit. The measurement volume was calibrated on each experimental day with 20 nM Rhodamine 6 G (Diffusion Coefficient, D, 2.8 $x10^{-10}$ m^2s^{-1}) in HPLC grade water. Exendin-4-TMR and Exendin-4-TMR-C16 were prepared in HBSS with or without 0.1% BSA in an 8-well Nunc™ Lab-tek™ chambered coverglass (No. 1.0 borosilicate glass bottom) with the measurement volume placed 200 µm above the coverslip bottom. Autocorrelation curves were modelled in Zen 2012 (Carl Zeiss, Jena) to describe a single 3D

Downloaded from molpharm.aspetjournals.org at ASPET Journals on April 20, 2024

Molecular Pharmacology Fast Forward. Published on July 27, 2021 as DOI: 10.1124/molpharm.121.000270
This article has not been copyedited and formatted. The final version may differ from this version.

diffusing component under free diffusion (Corriden 2014). To determine the average molecular brightness of the labelled peptide, measurement reads were reanalyzed by Photon Counting Histogram (PCH) analysis within Zen 2012 (Huang *et al.*, 2004). PCH analysis can quantify the average molecular brightness, photon counts per molecule, of a species and also provides a means to separate and quantify the concentration of two species which differ in their average molecular brightness. The laser beam profile was approximated to follow a 3D Gaussian distribution, measurement reads were binned at 20 µs, appropriate for fluorescent species in solution, and the first order correction was calculated daily following calibration with 20 nM Rhodamine 6 G.

2.22 *In vivo* study

Animals were maintained in specific pathogen-free facilities, with *ad lib* access to food (except prior to fasting studies) and water. Studies were regulated by the UK Animals (Scientific Procedures) Act 1986 of the U.K. and approved by Imperial College London (Project License PB7CFFE7A). Male C57Bl/6 mice (Charles River, UK) were fed a 60% high fat diet (D12492, Research Diets, USA) for 3 months prior to the study to induce obesity and glucose intolerance. The study began after an additional 1-week acclimatisation period during which mice were singly housed and received sham intra-peritoneal (IP) injections. Mice were randomly allocated to treatment, with average group weight confirmed to be similar post-randomisation. The study began at the beginning of the dark phase with a single dose of each agonist or vehicle, combined with an IP glucose tolerance test (IPGTT). Agonist was prepared in 20% glucose solution at a volume to provide the indicated weight-adjusted agonist dose and 2 g/kg glucose. Blood glucose was monitored before and at 20-min intervals after agonist/vehicle/glucose administration using a hand-held glucose meter. After 72 hours, the IPGTT was repeated at the beginning of the dark phase without further agonist administration. Food intake was assessed during the study by weighing of food at set intervals. Changes to body weight were also assessed at set intervals.

Downloaded from molpharm.aspetjournals.org at ASPET Journals on April 20, 2024

Molecular Pharmacology Fast Forward. Published on July 27, 2021 as DOI: 10.1124/molpharm.121.000270
This article has not been copyedited and formatted. The final version may differ from this version.

2.23 Experimental design and statistical analysis considerations

A preliminary finding that exendin-4-C16 shows reduced β-arrestin-2 recruitment compared to exendin-4 (Lucey *et al.*, 2020), gave us a reasonable expectation that the two ligands would display alterations to other aspects of their pharmacology. Therefore we adopted an approach in which we planned to perform at least 5 independent replicates for quantitative cell culture assays as recommended by some authorities (Curtis *et al.*, 2018). We did not perform a formal power calculation. In some instances, we observed more subtle differences between compounds that required additional repeats to gain confidence in the magnitude of the effects size, which were then performed to allow comparisons between assays evaluating similar phenomena (e.g. BRET *versus* TR-FRET assays). Animal experiments were performed with 7-8 mice/group without a formal power calculation, but on the basis of our prior experience in determining meaningful differences between GLP-1RAs. The investigators were not fully blinded for *in vivo* studies but did not have reference to treatment allocation whilst conducting experiments; *in vitro* experiments were unblinded. No mice were excluded from the analyses. In cell culture experiments, technical replicates were averaged so that each individual experiment was treated as one biological replicate. Quantitative data were analysed using Prism 8.0 (GraphPad Software). Dose responses were analysed using 3 or 4-parameter logistic fits, with constraints imposed as appropriate. Bias analyses were performed as described in Section 2.5. Statistical comparisons were made by t-test or ANOVA as appropriate, with paired or matched designs used depending on the experimental design. Mean ± standard error of mean (SEM), with individual replicates in some cases, are displayed throughout. Statistical significance was inferred if $p<0.05$, without ascribing additional levels of significance.

Downloaded from molpharm.aspetjournals.org at ASPET Journals on April 20, 2024

Molecular Pharmacology Fast Forward. Published on July 27, 2021 as DOI: 10.1124/molpharm.121.000270
This article has not been copyedited and formatted. The final version may differ from this version.

3 Results

3.1 Exendin-4-C16 is a G protein-biased ligand at GLP-1R

An exendin-4 analogue with a C16 diacid at the C-terminus with a GK linker, originally described in our earlier publication (Lucey *et al.*, 2020), was used in the present study and is referred to as "exendin-4-C16" (Figure 1A). Competition binding experiments with FITC-conjugated antagonist ligand exendin(9-39) in HEK293 cells stably expressing SNAP-GLP-1R (Fang, Chen, Pickford, *et al.*, 2020) indicated an approximately two-fold reduction in binding affinity for exendin-4-C16 compared to unmodified exendin-4 (Figure 1B, Table 1). A minor reduction in cAMP signalling potency that was not statistically significant was also observed (Figure 1C, Table 1). To investigate the possibility that exendin-4-C16 may display altered preference for coupling to intracellular effectors, i.e. biased agonism, we used nanoluciferase complementation to measure recruitment of mini-G_s (Wan *et al.*, 2018) and β-arrestin-2 (Dixon *et al.*, 2016) to the GLP-1R. This assay indicated that efficacy for β-arrestin-2 recruitment was particularly reduced with exendin-4-C16, with bias quantification using a standard approach (van der Westhuizen *et al.*, 2014) confirming preferential coupling to mini-G_s recruitment (Figure 1D, Table 1). β-arrestin-1 and β-arrestin-2 recruitment were also measured using the PathHunter assay, showing no evidence of divergence in isoform selectivity (Supplementary Figure 1A).

As these complementation assays measure effector recruitment but not activation, we also performed further experiments to detect ligand-induced conformational changes in G_s and β-arrestin-2. For the former we recorded dynamic changes in intermolecular BRET signal between GLP-1R tagged at the C-terminus with nanoluciferase and GFP-tagged nanobody 37 (Nb37), a genetically encoded intrabody that recognises and is recruited to active $G\alpha_s$ conformations (Irannejad *et al.*, 2013). For the latter we used an intramolecular β-arrestin-2 BRET sensor in which conformational changes lead to an increase in proximity between nanoluciferase at the N-terminus and CyOFP at the C-terminus (Oishi *et al.*, 2019); this phenomenon is typically thought to indicate transition to an "active" state that could

Downloaded from molpharm.aspetjournals.org at ASPET Journals on April 20, 2024

Molecular Pharmacology Fast Forward. Published on July 27, 2021 as DOI: 10.1124/molpharm.121.000270
This article has not been copyedited and formatted. The final version may differ from this version.

facilitate kinase activation (Nuber *et al.*, 2016), although this was not specifically determined in our study. These studies suggested reduced β-arrestin-2 conformational rearrangement with exendin-4-C16 but, interestingly, increased $G\alpha_s$ activation (Figure 1E, 1F, Supplementary Figure 1B), which could be a consequence of reduced β-arrestin-mediated desensitisation. This $G\alpha_s$ activation assay showed a low dynamic range but Ex4-C16 consistently showed a subtly increased response across all experimental repeats (Supplementary Figure 5B). Note that the apparent increase in $G\alpha_s$ activation is still compatible with a lack of difference in measured E_{max} for cAMP (Figure 1C), as adenylate cyclase activity may be saturated at sub-maximal activation of the cellular $G\alpha_s$ pool. Ligand pharmacology is summarised in the heatmap shown in Figure 1G, indicating how, at a 100 nM dose to achieve close to 100% receptor occupancy, G_s recruitment and activation are favoured compared to β-arrestin-2 responses with exendin-4-C16.

As G protein-directed agonism is now established as a means to improve GLP-1R-mediated insulinotropic efficacy by avoiding receptor desensitisation over prolonged stimulation periods (Jones *et al.*, 2018; Fremaux *et al.*, 2019; Fang, Chen, Pickford, *et al.*, 2020; Lucey *et al.*, 2020), we also treated INS-1 832/3 clonal beta cells (Hohmeier *et al.*, 2000) for both 1 and 16 hours with exendin-4 and exendin-4-C16 and measured cumulative insulin secretion. As expected, there was no difference in acute insulin release (Figure 1H), but the maximum response was increased with the -C16 ligand (Figure 1I, Table 1).

3.2 Exendin-4-C16 triggers slower GLP-1R internalisation compared to exendin-4

GLP-1R undergoes rapid agonist-induced internalisation (Widmann *et al.*, 1995), a process that is intrinsically linked to the spatial orchestration of intracellular signal generation (Fletcher *et al.*, 2018; Tomas *et al.*, 2019; Manchanda *et al.*, 2021). Both exendin-4 and exendin-4-C16 resulted in extensive endocytosis of surface-labelled SNAP-GLP-1R (Figure 2A). To quantify this process, we used high content time-lapse microscopy in which the translocation of surface-labelled SNAP-GLP-1R into the endocytic network is determined from the appearance an intracellular punctate distribution of fluorescent signal (Figure 2B,

Downloaded from molpharm.aspetjournals.org at ASPET Journals on April 20, 2024

Molecular Pharmacology Fast Forward. Published on July 27, 2021 as DOI: 10.1124/molpharm.121.000270
This article has not been copyedited and formatted. The final version may differ from this version.

Supplementary Figure 2A, Supplementary Video 1). Treatment with exendin-4 resulted in faster and more extensive appearance of fluorescent puncta at higher ligand concentrations. Notably, the number of puncta tended to reduce at later time-points with exendin-4 due to the coalescence in a perinuclear location where multiple punctate endosomal structures which could no longer be individually resolved.

We also used tetramethylrhodamine (TMR)-tagged conjugates of each ligand, with the fluorophore installed at position K12, previously shown to be well tolerated by exendin-4 (Clardy *et al.*, 2014; Jones *et al.*, 2018; Pickford *et al.*, 2020) and validated for GLP-1R binding by TR-FRET (Supplementary Figure 2B) and cAMP measurements (Supplementary Figure 2C), with the latter showing modest reductions in potency for both TMR-conjugates. Using the tetracycline-inducible T-REx system to modulate SNAP-GLP-1R expression (Fang, Chen, Manchanda, *et al.*, 2020), both fluorescent ligands were shown to bind specifically to the receptor and demonstrated extensive uptake into the endosomal compartment (Figure 2C).

3.3 Endosomal trafficking differences between exendin-4 and exendin-4-C16

To gain insights into ligand-induced GLP-1R movements to or from different subcellular compartments, we used time-resolved proximity-based energy transfer techniques, with both chemical (for FRET) or genetically encoded (for BRET) acceptors as localisation markers, providing complementary readouts. SNAP-GLP-1R labelled at the N-terminus with the lanthanide probe Lumi4-Tb can transfer energy to time-resolved FRET acceptors situated in the extracellular space or the endosomal lumen (Figure 3A). Diffusion-enhanced resonance energy transfer (DERET) was used to quantify movement of GLP-1R away from the cell surface as a reduction in signal transfer to fluorescein-containing extracellular buffer (Levoye *et al.*, 2015); this confirmed that GLP-1R internalisation was slower for exendin-4-C16 (Figure 3B, Supplementary Figure 3A). We developed a further assay in which the trafficking of GLP-1R to late endosomes / lysosomes was detected by energy transfer to the lysomotropic fluorescent dye LysoTracker-DND99 (Figure 3C). This suggested that exendin-

Downloaded from molpharm.aspetjournals.org at ASPET Journals on April 20, 2024

Molecular Pharmacology Fast Forward. Published on July 27, 2021 as DOI: 10.1124/molpharm.121.000270
This article has not been copyedited and formatted. The final version may differ from this version.

4-C16 treatment led to markedly less targeting of GLP-1R to this degradative compartment and, as this difference was more marked than for the internalisation reading by DERET, that this reflects a difference in post-endocytic targeting rather than simply less GLP-1R internalisation. In contrast, post-endocytic recycling of GLP-1R back to the plasma membrane, measured by time-resolved FRET (Fang, Chen, Pickford, *et al.*, 2020) between reemergent GLP-1R and Cy5-labelled antagonist analogue of exendin(9-39) (Ast *et al.*, 2020), was faster after treatment with exendin-4-C16 (Figure 3D). TR-FRET data are also summarised and statistically compared in Figure 3E.

Bystander BRET can be used to monitor the translocation of GPCRs within the endocytic network (Tiulpakov *et al.*, 2016). We observed a ligand-induced reduction in BRET signal when SNAP-GLP-1R tagged at the C-terminus with nanoluciferase was co-expressed with the plasma membrane marker KRAS-Venus; the effect was more pronounced with exendin-4 than with exendin-4-C16 (Figure 3F). A concomitant increase in BRET signal to Rab5-Venus was seen, indicating entry of the receptor into early endosomes (Figure 3G). The similar Rab5 BRET signal for each ligand in the face of apparently different GLP-1R internalisation rates might be reconciled by the observation that, after exendin-4-C16 treatment, a subtly reduced signal from Rab7-positive late endosomes was detected (Figure 3H), whereas a greater signal was recorded from Rab11-positive recycling endosomes (Figure 3I). This pattern is suggestive of preferential trafficking of GLP-1R towards a recycling pathway with exendin-4-C16 treatment, resulting in a reduced net rate of surface receptor loss. BRET results were broadly in accordance with results from the TR-FRET assays, although differences were generally smaller whilst remaining statistically significant (Figure 3J).

GLP-1R cAMP signalling was reported to originate from early endosomes as well as the plasma membrane (Girada *et al.*, 2017). As an indirect readout of this process, we monitored the redistribution of nanoluciferase-tagged mini-G_s to different subcellular compartments after agonist stimulation. A rapid increase in mini-G_s-to-KRAS (plasma membrane) BRET signal was apparent with both ligands (Figure 3K), but with a slightly

Downloaded from molpharm.aspetjournals.org at ASPET Journals on April 20, 2024

Molecular Pharmacology Fast Forward. Published on July 27, 2021 as DOI: 10.1124/molpharm.121.000270
This article has not been copyedited and formatted. The final version may differ from this version.

higher peak response with exendin-4 consistent with the higher efficacy displayed by this ligand for G protein recruitment (Figure 1D). A decline in signal at later time-points was observed with exendin-4 but not exendin-4-C16, which may result from more extensive β-arrestin-mediated steric hinderance or internalisation of GLP-1R with the former ligand. Interestingly, mini-G_s-to-Rab5 (early endosome) BRET signal amplitude was considerably reduced for exendin-4-C16 (Figure 3K), despite the fact that the receptor localisation in the Rab5 compartment was similar for both ligands (Figure 3G).

These data indicate that C-terminal acylation alters the trafficking profile of exendin-4, favouring GLP-1R sorting towards a recycling rather than degradative pathway. The observation that mini-G_s protein recruitment to early endosomes was reduced with exendin-4-C16, yet this ligand shows higher efficacy for sustained insulin secretion, suggests that signalling from early endosomes may not be a dominant mechanism for prolonged signalling with GLP-1R under pharmacological conditions, at least with exendin-4 derived GLP-1R agonists.

3.4 Acylation affects the interaction of the exendin-4 peptide with the plasma membrane

Several studies report an interaction of GLP-1R agonist peptides with model membranes, typically resulting in enhanced stability of the helical secondary structure (Thornton and Gorenstein, 1994; Neidigh *et al.*, 2001; NH Andersen *et al.*, 2002; Fox *et al.*, 2009). Acylation of glucagon-like peptide-2 increases its tendency to interact with lipid bilayers (Trier *et al.*, 2014). Similarly, the C16 chain of exendin-4-C16 might promote selective engagement with membrane regions dependent on local hydrophobicity. We performed confocal microscopy of FITC conjugates of exendin-4 and exendin-4-C16 bound to giant unilamellar vesicles (GUVs), prepared via electroformation. Both FITC ligands were conjugated at position K12, as for the equivalent TMR conjugates, and retained GLP-1R binding properties (Supplementary Figure 4A) and cAMP signalling (Supplementary Figure 4B). When the acylated compound was present in the sample, clear fluorescence

Downloaded from molpharm.aspetjournals.org at ASPET Journals on April 20, 2024

Molecular Pharmacology Fast Forward. Published on July 27, 2021 as DOI: 10.1124/molpharm.121.000270
This article has not been copyedited and formatted. The final version may differ from this version.

accumulation was seen on the membrane surface, in contrast to the non-acylated compound where no accumulation was seen (Figure 4A). This demonstrates that the presence of the C16 acyl chain promotes insertion of the molecule into model lipid bilayers.

To establish whether this phenomenon is relevant to living cells, we measured FRET between FITC-ligands and the plasma membrane of T-Rex-SNAP-GLP-1R cells labelled with the solvatochromic probe NR12S (Kucherak *et al.*, 2010). The excitation spectrum of NR12S is well matched to the emission spectrum of FITC and its emission spectrum is polarity-sensitive, potentially allowing discrimination of interactions occurring in membrane domains with different degrees of liquid order, e.g. lipid rafts *versus* non-raft regions. The NR12S spectra obtained from excitation of FITC ligands incubated with NR12S-labelled cells showed an increase in maximum FRET signal without any significant spectral shift (Figure 4B). Similar findings were observed with or without GLP-1R expression in the same cell system (Figure 4B). This suggests that exendin-4-C16 may indeed interact with cell membranes to a greater extent than does exendin-4, but does not provide evidence that this directs the ligand to interact with specific GLP-1R subpopulations situated in membrane nanodomains with different degrees of liquid order.

We also investigated the possibility of ligand-specific GLP-1R cAMP signal localisation using the targeted cAMP FRET biosensor AKAP79-CUTie (Surdo *et al.*, 2017). AKAP79 is a protein kinase A (PKA) anchoring protein that is typically situated in membrane rafts by virtue of its palmitoylation (Delint-Ramirez *et al.*, 2011). FRET imaging indicated similar kinetics for nanodomain-specific cAMP production with a saturating concentration of exendin-4 and exendin-4-C16 (Figure 4C). Comparisons of ligand potencies for AKAP79-CUTie *versus* total cAMP measured by HTRF indicated that exendin-4-induced cAMP signalling is more constrained to AKAP79-marked nanodomains than for exendin-4-C16 (Figure 4D, Supplementary Figure 4C). On the other hand, pre-treatment with methyl-β-cyclodextrin (MβCD) to sequester cholesterol and disrupt membrane nanodomain structure (Mahammad and Parmryd, 2015) disproportionately reduced cAMP production by exendin-4-C16 compared to exendin-4 (Figure 4E). This might result from the lower G protein

Downloaded from molpharm.aspetjournals.org at ASPET Journals on April 20, 2024

Molecular Pharmacology Fast Forward. Published on July 27, 2021 as DOI: 10.1124/molpharm.121.000270
This article has not been copyedited and formatted. The final version may differ from this version.

recruitment efficacy of exendin-4-C16 meaning that its ability to generate cAMP signals is more susceptible to uncoupling of G proteins from receptors as a result of disruption of membrane structure (Mystek *et al.*, 2016). Similarly, exendin-4-C16-induced GLP-1R endocytosis, measured by TR-FRET, was more substantially affected by MβCD treatment than exendin-4 (Figure 4F).

To gain further insights into how exendin-4 and exendin-4-C16 interact with GLP-1R at the plasma membrane, we used NR12S as a FRET acceptor for the N-terminally SNAP-tagged GLP-1R labelled with Lumi-4-Tb, monitoring dynamic changes in TR-FRET signal with each ligand over time indicative of movement of the receptor extracellular domain (ECD) relative to the plasma membrane (Figure 4G). A similar principle has been used previously to monitor epidermal growth factor receptor (EGFR) conformational shifts by FRET microscopy (Ziomkiewicz *et al.*, 2013). Here, both ligands led to clear increases in TR-FRET signal across a wide concentration range. Efficacy was reduced with exendin-4-C16 (Figure 4G), in keeping with lower efficacy measurements for intracellular responses including recruitment of mini-G_s and β-arrestin-2 (see Figure 1), although an increase in potency was observed. The implications of these responses are not clear, as they could reflect differences in ECD movement, known to be a feature of GLP-1R activation as determined from structural and computational studies (J Zhang *et al.*, 2019; Wu *et al.*, 2020), but ligand-induced effects on membrane architecture cannot be ruled out.

3.5 Interaction of exendin-4-C16 with albumin and *in vivo* efficacy

The classical benefit of peptide acylation is to promote reversible binding to albumin in the circulation, thereby avoiding renal elimination. We previously showed that exendin-4-C16 and related analogues are >97% bound to proteins in human and mouse plasma (Lucey *et al.*, 2020). In the present study we performed fluorescence correlation spectroscopy (FCS) to measure the interaction of both TMR-conjugated peptides with bovine serum albumin (BSA) (Figure 5A-C). All traces could be fitted to a 1x3D free diffusion model, indicating there is a single diffusing component. Diffusion coefficients for exendin-4-TMR and exendin-

Downloaded from molpharm.aspetjournals.org at ASPET Journals on April 20, 2024

Molecular Pharmacology Fast Forward. Published on July 27, 2021 as DOI: 10.1124/molpharm.121.000270
This article has not been copyedited and formatted. The final version may differ from this version.

4-TMR-C16, tested at a range of concentrations between 2.5 and 20 nM, were similar in the absence of BSA (Figure 5B). However, diffusion of exendin-4-TMR-C16 was markedly slowed in the presence of BSA, indicative of formation of peptide-albumin complexes. (Figure 5A, 5B). Exendin-4-TMR-C16 measurement reads were reanalysed by photon counting histogram (PCH) analysis with all reads fitting to a single-species PCH fit and the reported average molecular brightness unaffected by the addition of BSA (Figure 5C). These results support our interpretation of a slowing of diffusion coefficient as a result of exendin-4-TMR-C16 interaction with BSA rather than an accumulation of peptide, which would have resulted in an increase in average molecular brightness.

Finally, the metabolic effects of exendin-4 and exendin-4-C16 were compared in mice in which glucose intolerance was first induced by high fat feeding for 2 months prior to the study. Exendin-4-C16 was previously shown to be detectable in plasma 72 hours after dosing (Lucey *et al.*, 2020). Therefore, the effect of a single administration of each ligand, at two separate doses, was assessed. Both doses of exendin-4-C16 led to greater suppression of food intake and weight loss throughout the dosing period (Figure 5D, 5E). Moreover, both doses of the acylated ligand exerted a larger anti-hyperglycaemic effect in an intra-peritoneal glucose tolerance test performed 72 hours after dosing (Figure 5F).

Downloaded from molpharm.aspetjournals.org at ASPET Journals on April 20, 2024

Molecular Pharmacology Fast Forward. Published on July 27, 2021 as DOI: 10.1124/molpharm.121.000270
This article has not been copyedited and formatted. The final version may differ from this version.

4 Discussion

This study demonstrates how C-terminal acylation of exendin-4 affects several GLP-1R pharmacological properties that are relevant to its therapeutic effect. Whilst exendin-4-C16 showed minimal reduction in cAMP signalling potency, marked differences were observed for recruitment of key intracellular effectors and trafficking responses, which led to increased insulin secretion with prolonged incubations. We also evaluated the effect of peptide acylation on binding to membranes and albumin to more comprehensively describe the differences between these ligands. Overall, our study highlights the breadth of pharmacological parameters than can be affected by peptide acylation.

This work was prompted by our earlier observation that C-terminal acylation of biased GLP-1RAs based on exendin-4 results in reduced recruitment efficacy for β-arrestin and mini-G protein (Lucey *et al.*, 2020). The present study confirms this observation, with a 60% reduction in maximum response recorded for β-arrestin-2 recruitment by nanoBiT complementation with exendin-4-C16. Whilst mini-G_s recruitment was also reduced, the impact on β-arrestin-2 recruitment was greater, with biased agonism confirmed by the operational model approach and on the basis of efficacy differences (Onaran *et al.*, 2017). We note that this does not indicate that the ligands show opposing preference for G protein- *versus* β-arrestin- "favouring" GLP-1R conformations; the observed bias more likely results from the fact that β-arrestin responses appear to be more susceptible to reductions in GLP-1R efficacy than do G protein responses. Indeed, our data add to the growing body of evidence that G protein-favouring biased GLP-1RAs typically show reduced efficacy for recruitment of both G proteins and β-arrestins (Lucey *et al.*, 2020; Pickford *et al.*, 2020; Fang, Chen, Pickford, *et al.*, 2020). However, using a novel Nb37-based BRET approach to monitor activation of endogenous G proteins close to GLP-1R, we demonstrate here that exendin-4-C16 shows increases in $G\alpha_s$ activation in spite of its lower mini-G_s recruitment efficacy. This could reflect an inherent difference in ability of exendin-4-C16 to activate $G\alpha_s$ in spite of reduced recruitment. However, we suspect the real reason is that the activation assay is more susceptible to normal regulatory processes, such as steric hindrance by β-

Downloaded from molpharm.aspetjournals.org at ASPET Journals on April 20, 2024

arrestin recruitment, which fail to displace mini-G responses due to the highly stable nature of the GPCR-mini-G complexes (Carpenter and Tate, 2016). Whilst the dynamic range of this assay was low in our hands, making it challenging to apply to higher throughput screening efforts or to concentration responses, it could be adapted by the use of alternative fluorophores with greater signal separation from the nanoluciferase emission peak (Dale *et al.*, 2019) or using complementation approaches (Inoue *et al.*, 2019). Other approaches to monitor G protein activation have typically required overexpression of tagged G protein subunits (Masuho *et al.*, 2015; Inoue *et al.*, 2019; Zhao *et al.*, 2020; Olsen *et al.*, 2020), which may not totally replicate the physiological setting, although corroboration using these approaches would be useful for validation.

In line with other studies showing that lower efficacy biased GLP-1RAs tend to induce slower GLP-1R endocytosis (Jones *et al.*, 2018; Fremaux *et al.*, 2019; Lucey *et al.*, 2020; Willard *et al.*, 2020), we observed that GLP-1R internalisation was reduced with exendin-4-C16 compared to exendin-4. The automated microscopy approach we used to demonstrate this has certain advantages over lower throughput methods, by allowing responses to a wide range of ligands or, in this case, ligand concentrations to be monitored in parallel across several FOVs, characterising ligand effects in more detail and with greater statistical robustness. However, this method is unable to discriminate between GLP-1R clustering at the plasma membrane *versus* bona fide endocytosis events, although these are intrinsically linked, with the former occurring rapidly after ligand stimulation as a precursor to uptake into clathrin-coated vesicles (Buenaventura *et al.*, 2019). The system could be adapted for use with alternative fluorescence approaches to monitor internalisation, e.g. using pH-sensitive SNAP-labelling fluorophores (Martineau *et al.*, 2017).

We also applied a series of complementary proximity-based techniques based on both BRET and FRET to monitor GLP-1R redistribution between the plasma membrane and different endosomal compartments. Monitoring GLP-1R disappearance from the plasma membrane by DERET has been widely applied (Roed *et al.*, 2014; Jones *et al.*, 2018), and the use of the cleavable BG-Lumi4-Tb to monitor GLP-1R recycling in combination with a

Downloaded from molpharm.aspetjournals.org at ASPET Journals on April 20, 2024

Molecular Pharmacology Fast Forward. Published on July 27, 2021 as DOI: 10.1124/molpharm.121.000270
This article has not been copyedited and formatted. The final version may differ from this version.

fluorescent antagonist ligand was recently described by our group (Pickford *et al.*, 2020). We extended this approach here to detect GLP-1R translocation to late endosomes and lysosomes marked by the lysomotropic dye LysoTracker, facilitated by the spectral overlap of one of the Tb emission peaks with the excitation spectrum of LysoTracker DND99. In principle, a similar approach could be trialled with other fluorescent markers that accumulate in different subcellular compartments. Using a nanoluciferase tag at the GLP-1R C-terminus, we were also able to obtain BRET measurements of GLP-1R redistribution to early, late and recycling endosomes that corroborate the TR-FRET responses. This approach has been used recently to study the trafficking profiles of GLP-1R mono-agonists and dual GLP-1R/GIPR co-agonists (Fletcher *et al.*, 2018; Novikoff *et al.*, 2021), albeit using Renilla luciferase rather than the nanoluciferase we used in our study. The rank order of ligand-induced changes was consistent for "matched" TR-FRET and BRET approaches, with exendin-4-C16 showing reduced GLP-1R internalisation and lysosomal accumulation, but faster recycling. In our hands the TR-FRET approach resulted in clearer discrimination between ligand responses, which could reflect cell model differences, influence of the C-terminal NLuc tag for BRET, or assay/instrument sensitivity.

Importantly, we also observed differences in mini-G_s recruitment to plasma membrane *versus* early endosomes using the nanoBRET approach, providing some insight into compartmentalisation of GLP1-R signalling. Here, plasma membrane mini-G_s recruitment was somewhat reduced for exendin-4-C16 compared to exendin-4, which is compatible with results from our nanoBiT complementation assay demonstrating reduced global mini-G_s recruitment efficacy for this ligand. However, recruitment of mini-G_s to Rab5-positive early endosomes was reduced to an even greater extent, which can be at least partly explained by the reduced rate of internalisation with this ligand, although differences in ability to maintain GLP-1R activation once internalised could also contribute. Indeed, the GLP-1R-Rab5 BRET signal was only marginally reduced with exendin-4-C16 *versus* exendin-4, whereas the mini-G_s-Rab5 BRET response showed larger differences between ligands. However, differences in luciferase/fluorophore configuration between assays, as

Downloaded from molpharm.aspetjournals.org at ASPET Journals on April 20, 2024

well as unknown effects of mini-G_s overexpression on GLP-1R pharmacology mean that further work will be needed to fully explain this observation. GLP-1R has been reported to generate signals from the endosomal compartment (Kuna *et al.*, 2013; Roed *et al.*, 2015; Girada *et al.*, 2017; Fletcher *et al.*, 2018), in line with many other GPCRs (Vilardaga *et al.*, 2014), and this phenomenon is frequently claimed to be a mechanism for sustained cAMP signalling. However, while our results corroborate the existence of GLP-1R-associated endosomal signalling, they also suggest that sustained GLP-1R signalling, as indicated by cumulative insulin secretion over pharmacologically relevant timescales, is actually greater with the ligand (exendin-4-C16) with a reduced tendency to recruit mini-G_s to Rab5-positive endosomes. This raises questions about the relative therapeutic importance of maintaining an adequate pool of surface GLP-1Rs during prolonged stimulations *versus* aiming for maximal endosomal receptor activation.

The structural basis for the modified GLP-1R activation profile with exendin-4-C16 is not clear. The C-terminus of exendin-4, whilst not required for GLP-1R activation (Lee *et al.*, 2018), plays an important role in GLP-1R binding (Doyle *et al.*, 2003). Installation of a large acyl chain at the peptide C-terminus could potentially interfere with ligand binding. We observed a modest reduction in GLP-1R binding affinity, in keeping with this possibility. However, receptor activation efficacy was also reduced. Interestingly, the C-terminus of exendin-4 may be required to facilitate formation of high order GLP-1R oligomers through interaction with neighbouring GLP-1R protomers in *trans* (Koole *et al.*, 2017). GLP-1R oligomerisation is reported to be required for full signalling responses (Harikumar *et al.*, 2012). A further possibility is that the acyl chain could interact with the plasma membrane in a specific manner that interferes with GLP-1R activation. We found here that a fluorescently labelled exendin-4-C16 does indeed form interactions with model membranes whereas the equivalently labelled non-acylated exendin-4 does not. Corresponding measurements from living cells also suggested greater membrane interactions with the acylated ligand but did not support the possibility of localised activation of GLP-1R subpopulations situated in particular plasma membrane nanodomains.

Downloaded from molpharm.aspetjournals.org at ASPET Journals on April 20, 2024

Molecular Pharmacology Fast Forward. Published on July 27, 2021 as DOI: 10.1124/molpharm.121.000270
This article has not been copyedited and formatted. The final version may differ from this version.

As differential ability of ligands to stabilise active GLP-1R conformations are a further potential explanation for the ligand signalling efficacy differences, we devised a strategy to monitor movements between the receptor ECD and the plasma membrane, finding efficacy reductions with exendin-4-C16 that matched the reduced intracellular signalling responses also observed with this ligand. This approach may be more widely useful as a conformational sensor for other GPCRs, although it lacks the ability to detect changes at the receptor intracellular face that are needed to provide insights into conformational changes required for G protein interactions.

There are a number of limitations with our study. Firstly, we investigated the effects of a single type of C16 diacid acyl chain, and our results are not necessarily extrapolable to GLP-1R agonists with different acyl chain lengths or acyl monoacids. Secondly, the majority of studies were performed in heterologous cell lines with overexpression of tagged GLP-1R constructs, which could influence the pharmacology. Whilst numerous studies have demonstrated that biased agonism and trafficking assessments in heterologous systems reliable predict insulin secretory and other key physiological effects of biased GLP-1RAs *in vivo*, the field would benefit from further efforts to study behaviours of endogenous GLP-1R in beta cells and cell types with native GLP-1R expression.

In summary, beyond the expected effects on binding to albumin, C-terminal acylation of exendin-4 led to changes in multiple pharmacological parameters relevant to downstream GLP-1R responses. These observations are more broadly relevant to drug discovery at peptide GPCRs for which ligand acylation is a valid approach to improve pharmacokinetics.

Downloaded from molpharm.aspetjournals.org at ASPET Journals on April 20, 2024

Molecular Pharmacology Fast Forward. Published on July 27, 2021 as DOI: 10.1124/molpharm.121.000270
This article has not been copyedited and formatted. The final version may differ from this version.

Author contributions

Participated in research design: Lucey, Wang, Goulding, Minnion, Elani, Briddon, Bloom, Tomas, Jones.

Conducted experiments: Lucey, Ashik, Marzook, Wang, Goulding, Elani, Jones.

Contributed new reagents or analytic tools: Marzook, Oishi, Broichhagen, Hodson, Jockers.

Performed data analysis: Lucey, Ashik, Goulding, Elani, Jones.

Wrote or contributed to the writing of the manuscript: Lucey, Ashik, Marzook, Wang, Goulding, Oishi, Broichhagen, Hodson, Minnion, Elani, Jockers, Briddon, Bloom, Tomas, Jones.

Downloaded from molpharm.aspetjournals.org at ASPET Journals on April 20, 2024

Molecular Pharmacology Fast Forward. Published on July 27, 2021 as DOI: 10.1124/molpharm.121.000270
This article has not been copyedited and formatted. The final version may differ from this version.

5 References

Andersen A, Lund A, Knop FK, and Vilsbøll T (2018) Glucagon-like peptide 1 in health and disease. *Nat Rev Endocrinol* **14**:390–403.

Andersen NH, Brodsky Y, Neidigh JW, and Prickett KS (2002) Medium-dependence of the secondary structure of exendin-4 and glucagon-like-peptide-1. *Bioorg Med Chem* **10**:79–85.

Ast J, Arvaniti A, Fine NHF, Nasteska D, Ashford FB, Stamataki Z, Koszegi Z, Bacon A, Jones BJ, Lucey MA, Sasaki S, Brierley DI, Hastoy B, Tomas A, D'Agostino G, Reimann F, Lynn FC, Reissaus CA, Linnemann AK, D'Este E, Calebiro D, Trapp S, Johnsson K, Podewin T, Broichhagen J, and Hodson DJ (2020) Super-resolution microscopy compatible fluorescent probes reveal endogenous glucagon-like peptide-1 receptor distribution and dynamics. *Nat Commun* **11**:467.

Buenaventura T, Bitsi S, Laughlin WE, Burgoyne T, Lyu Z, Oqua AI, Norman H, McGlone ER, Klymchenko AS, Corrêa IR, Walker A, Inoue A, Hanyaloglu A, Grimes J, Koszegi Z, Calebiro D, Rutter GA, Bloom SR, Jones B, and Tomas A (2019) Agonist-induced membrane nanodomain clustering drives GLP-1 receptor responses in pancreatic beta cells. *PLoS Biol* **17**:e3000097.

Carpenter B, and Tate CG (2016) Engineering a minimal G protein to facilitate crystallisation of G protein-coupled receptors in their active conformation. *Protein Eng Des Sel* **29**:583–594.

Clardy SM, Keliher EJ, Mohan JF, Sebas M, Benoist C, Mathis D, and Weissleder R (2014) Fluorescent exendin-4 derivatives for pancreatic β-cell analysis. *Bioconjug Chem* **25**:171–177.

Corriden R, Kilpatrick LE, Kellam B, Briddon SJ, and Hill SJ (2014) Kinetic analysis of antagonist-occupied adenosine-A3 receptors within membrane microdomains of individual cells provides evidence of receptor dimerization and allosterism. *FASEB J* **28**:4211–4222.

Curtis MJ, Alexander S, Cirino G, Docherty JR, George CH, Giembycz MA, Hoyer D, Insel PA, Izzo AA, Ji Y, MacEwan DJ, Sobey CG, Stanford SC, Teixeira MM, Wonnacott S, and Ahluwalia A (2018) Experimental design and analysis and their reporting II: updated and simplified guidance for authors and peer reviewers. *Br J Pharmacol* **175**:987–993.

Dale NC, Johnstone EKM, White CW, and Pfleger KDG (2019) NanoBRET: The Bright Future of Proximity-Based Assays. *Front Bioeng Biotechnol* **7**:56, Frontiers.

Delint-Ramirez I, Willoughby D, Hammond GRV, Hammond GVR, Ayling LJ, and Cooper DMF (2011) Palmitoylation targets AKAP79 protein to lipid rafts and promotes its regulation of calcium-sensitive adenylyl cyclase type 8. *J Biol Chem* **286**:32962–32975.

Dixon AS, Schwinn MK, Hall MP, Zimmerman K, Otto P, Lubben TH, Butler BL, Binkowski BF, Machleidt T, Kirkland TA, Wood MG, Eggers CT, Encell LP, and Wood KV (2016) NanoLuc Complementation Reporter Optimized for Accurate Measurement of Protein Interactions in Cells. *ACS Chem Biol* **11**:400–408.

Doyle ME, Theodorakis MJ, Holloway HW, Bernier M, Greig NH, and Egan JM (2003) The importance of the nine-amino acid C-terminal sequence of exendin-4 for binding to the GLP-1 receptor and for biological activity. *Regul Pept* **114**:153–158.

Downloaded from molpharm.aspetjournals.org at ASPET Journals on April 20, 2024

Fang Z, Chen S, Manchanda Y, Bitsi S, Pickford P, David A, Shchepinova MM, Corrêa IR Jr, Hodson DJ, Broichhagen J, Tate EW, Reimann F, Salem V, Rutter GA, Tan T, Bloom SR, Tomas A, and Jones B (2020) Ligand-Specific Factors Influencing GLP-1 Receptor Post-Endocytic Trafficking and Degradation in Pancreatic Beta Cells. *Int J Mol Sci* **21**:8404, Multidisciplinary Digital Publishing Institute.

Fang Z, Chen S, Pickford P, Broichhagen J, Hodson DJ, Corrêa IR, Kumar S, Görlitz F, Dunsby C, French PMW, Rutter GA, Tan T, Bloom SR, Tomas A, and Jones B (2020) The Influence of Peptide Context on Signaling and Trafficking of Glucagon-like Peptide-1 Receptor Biased Agonists. *ACS Pharmacol Transl Sci* **3**:345–360.

Fletcher MM, Halls ML, Zhao P, Clydesdale L, Christopoulos A, Sexton PM, and Wootten D (2018) Glucagon-like peptide-1 receptor internalisation controls spatiotemporal signalling mediated by biased agonists. *Biochem Pharmacol* **156**:406–419.

Fox CB, Wayment JR, Myers GA, Endicott SK, and Harris JM (2009) Single-molecule fluorescence imaging of peptide binding to supported lipid bilayers. *Anal Chem* **81**:5130–5138.

Fremaux J, Venin C, Mauran L, Zimmer R, Koensgen F, Rognan D, Bitsi S, Lucey MA, Jones B, Tomas A, Guichard G, and Goudreau SR (2019) Ureidopeptide GLP-1 analogues with prolonged activity in vivo via signal bias and altered receptor trafficking. *Chem Sci* **10**:9872–9879.

Girada SB, Kuna RS, Bele S, Zhu Z, Chakravarthi NR, Dimarchi RD, and Mitra P (2017) Gαs regulates Glucagon-Like Peptide 1 Receptor-mediated cyclic AMP generation at Rab5 endosomal compartment. *Mol Metab* **6**:1173–1185.

Graaf C de, Donnelly D, Wootten D, Lau J, Sexton PM, Miller LJ, Ahn J-M, Liao J, Fletcher MM, Yang D, Brown AJH, Zhou C, Deng J, and Wang M-W (2016) Glucagon-Like Peptide-1 and Its Class B G Protein-Coupled Receptors: A Long March to Therapeutic Successes. *Pharmacol Rev* **68**:954–1013.

Guariguata L, Whiting DR, Hambleton I, Beagley J, Linnenkamp U, and Shaw JE (2014) Global estimates of diabetes prevalence for 2013 and projections for 2035. *Diabetes Res Clin Pract* **103**:137–149.

Harikumar KG, Wootten D, Pinon DI, Koole C, Ball AM, Furness SGB, Graham B, Dong M, Christopoulos A, Miller LJ, and Sexton PM (2012) Glucagon-like peptide-1 receptor dimerization differentially regulates agonist signaling but does not affect small molecule allostery. *Proc Natl Acad Sci USA* **109**:18607–18612, National Academy of Sciences.

Hohmeier HE, Mulder H, Chen G, Henkel-Rieger R, Prentki M, and Newgard CB (2000) Isolation of INS-1-derived cell lines with robust ATP-sensitive K+ channel-dependent and -independent glucose-stimulated insulin secretion. *Diabetes* **49**:424–430.

Huang B, Perroud TD, and Zare RN (2004) Photon counting histogram: one-photon excitation. *Chemphyschem* **5**:1523–1531.

Inoue A, Raimondi F, Kadji FMN, Singh G, Kishi T, Uwamizu A, Ono Y, Shinjo Y, Ishida S, Arang N, Kawakami K, Gutkind JS, Aoki J, and Russell RB (2019) Illuminating G-Protein-Coupling Selectivity of GPCRs. *Cell* **177**:1933–1947.e25.

Downloaded from molpharm.aspetjournals.org at ASPET Journals on April 20, 2024

Irannejad R, Tomshine JC, Tomshine JR, Chevalier M, Mahoney JP, Steyaert J, Rasmussen SGF, Sunahara RK, El-Samad H, Huang B, and Zastrow von M (2013) Conformational biosensors reveal GPCR signalling from endosomes. *Nature* **495**:534–538.

Jaccard N, Griffin LD, Keser A, Macown RJ, Super A, Veraitch FS, and Szita N (2014) Automated method for the rapid and precise estimation of adherent cell culture characteristics from phase contrast microscopy images. *Biotechnol Bioeng* **111**:504–517.

Jones B, Buenaventura T, Kanda N, Chabosseau P, Owen BM, Scott R, Goldin R, Angkathunyakul N, Corrêa IR, Bosco D, Johnson PR, Piemonti L, Marchetti P, Shapiro AMJ, Cochran BJ, Hanyaloglu AC, Inoue A, Tan T, Rutter GA, Tomas A, and Bloom SR (2018) Targeting GLP-1 receptor trafficking to improve agonist efficacy. *Nat Commun* **9**:1602, Nature Publishing Group.

Kenakin T, Watson C, Muniz-Medina V, Christopoulos A, and Novick S (2012) A simple method for quantifying functional selectivity and agonist bias. *ACS Chem Neurosci* **3**:193–203.

Knudsen LB, and Lau J (2019) The Discovery and Development of Liraglutide and Semaglutide. *Front Endocrinol (Lausanne)* **10**:155.

Kolterman OG, Buse JB, Fineman MS, Gaines E, Heintz S, Bicsak TA, Taylor K, Kim D, Aisporna M, Wang Y, and Baron AD (2003) Synthetic exendin-4 (exenatide) significantly reduces postprandial and fasting plasma glucose in subjects with type 2 diabetes. *J Clin Endocrinol Metab* **88**:3082–3089.

Koole C, Reynolds CA, Mobarec JC, Hick C, Sexton PM, and Sakmar TP (2017) Genetically encoded photocross-linkers determine the biological binding site of exendin-4 peptide in the N-terminal domain of the intact human glucagon-like peptide-1 receptor (GLP-1R). *J Biol Chem* **292**:7131–7144.

Kucherak OA, Oncul S, Darwich Z, Yushchenko DA, Arntz Y, Didier P, Mély Y, and Klymchenko AS (2010) Switchable nile red-based probe for cholesterol and lipid order at the outer leaflet of biomembranes. *J Am Chem Soc* **132**:4907–4916.

Kuna RS, Girada SB, Asalla S, Vallentyne J, Maddika S, Patterson JT, Smiley DL, Dimarchi RD, and Mitra P (2013) Glucagon-like peptide-1 receptor-mediated endosomal cAMP generation promotes glucose-stimulated insulin secretion in pancreatic β-cells. *Am J Physiol Endocrinol Metab* **305**:E161–70.

Lau J, Bloch P, Schäffer L, Pettersson I, Spetzler J, Kofoed J, Madsen K, Knudsen LB, McGuire J, Steensgaard DB, Strauss HM, Gram DX, Knudsen SM, Nielsen FS, Thygesen P, Reedtz-Runge S, and Kruse T (2015) Discovery of the Once-Weekly Glucagon-Like Peptide-1 (GLP-1) Analogue Semaglutide. *J Med Chem* **58**:7370–7380.

Lee JG, Ryu JH, Kim S-M, Park M-Y, Kim S-H, Shin YG, Sohn J-W, Kim HH, Park Z-Y, Seong JY, and Kim JI (2018) Replacement of the C-terminal Trp-cage of exendin-4 with a fatty acid improves therapeutic utility. *Biochem Pharmacol* **151**:59–68.

Levoye A, Zwier JM, Jaracz-Ros A, Klipfel L, Cottet M, Maurel D, Bdioui S, Balabanian K, Prézeau L, Trinquet E, Durroux T, and Bachelerie F (2015) A Broad G Protein-Coupled Receptor Internalization Assay that Combines SNAP-Tag Labeling, Diffusion-Enhanced Resonance Energy Transfer, and a Highly Emissive Terbium Cryptate. *Front Endocrinol (Lausanne)* **6**:167.

Downloaded from molpharm.aspetjournals.org at ASPET Journals on April 20, 2024

Lucey M, Pickford P, Bitsi S, Minnion J, Ungewiss J, Schoeneberg K, Rutter GA, Bloom SR, Tomas A, and Jones B (2020) Disconnect between signalling potency and in vivo efficacy of pharmacokinetically optimised biased glucagon-like peptide-1 receptor agonists. *Mol Metab* **37**:100991.

Mahammad S, and Parmryd I (2015) Cholesterol depletion using methyl-β-cyclodextrin. *Methods Mol Biol* **1232**:91–102.

Malm-Erjefält M, Bjørnsdottir I, Vanggaard J, Helleberg H, Larsen U, Oosterhuis B, van Lier JJ, Zdravkovic M, and Olsen AK (2010) Metabolism and excretion of the once-daily human glucagon-like peptide-1 analog liraglutide in healthy male subjects and its in vitro degradation by dipeptidyl peptidase IV and neutral endopeptidase. *Drug Metab Dispos* **38**:1944–1953.

Manchanda Y, Bitsi S, Kang Y, Jones B, and Tomas A (2021) Spatiotemporal control of GLP-1 receptor activity. *Current Opinion in Endocrine and Metabolic Research* **16**:19–27, Elsevier.

Martineau M, Somasundaram A, Grimm JB, Gruber TD, Choquet D, Taraska JW, Lavis LD, and Perrais D (2017) Semisynthetic fluorescent pH sensors for imaging exocytosis and endocytosis. *Nat Commun* **8**:1412–10, Nature Publishing Group.

Masuho I, Ostrovskaya O, Kramer GM, Jones CD, Xie K, and Martemyanov KA (2015) Distinct profiles of functional discrimination among G proteins determine the actions of G protein-coupled receptors. *Sci Signal* **8**:ra123–ra123, American Association for the Advancement of Science.

Mystek P, Dutka P, Tworzydło M, Dziedzicka-Wasylewska M, and Polit A (2016) The role of cholesterol and sphingolipids in the dopamine D1 receptor and G protein distribution in the plasma membrane. *Biochim Biophys Acta* **1861**:1775–1786.

Neidigh JW, Fesinmeyer RM, Prickett KS, and Andersen NH (2001) Exendin-4 and glucagon-like-peptide-1: NMR structural comparisons in the solution and micelle-associated states. *Biochemistry* **40**:13188–13200.

Novikoff A, O'Brien SL, Bernecker M, Grandl G, Kleinert M, Knerr PJ, Stemmer K, Klingenspor M, Zeigerer A, DiMarchi R, Tschöp MH, Finan B, Calebiro D, and Müller TD (2021) Spatiotemporal GLP-1 and GIPR receptor signaling and trafficking/recycling dynamics induced by selected receptor mono- and dual-agonists. *Mol Metab* 101181.

Nuber S, Zabel U, Lorenz K, Nuber A, Milligan G, Tobin AB, Lohse MJ, and Hoffmann C (2016) β-Arrestin biosensors reveal a rapid, receptor-dependent activation/deactivation cycle. *Nature* **531**:661–664.

Oishi A, Dam J, and Jockers R (2019) β-Arrestin-2 BRET Biosensors Detect Different β-Arrestin-2 Conformations in Interaction with GPCRs. *ACS Sens* acssensors.9b01414.

Olsen RHJ, DiBerto JF, English JG, Glaudin AM, Krumm BE, Slocum ST, Che T, Gavin AC, McCorvy JD, Roth BL, and Strachan RT (2020) TRUPATH, an open-source biosensor platform for interrogating the GPCR transducerome. *Nat Chem Biol* **16**:841–849, Nature Publishing Group.

Onaran HO, Ambrosio C, Uğur Ö, Madaras Koncz E, Grò MC, Vezzi V, Rajagopal S, and Costa T (2017) Systematic errors in detecting biased agonism: Analysis of current

Downloaded from molpharm.aspetjournals.org at ASPET Journals on April 20, 2024

methods and development of a new model-free approach. *Sci Rep* **7**:44247, Nature Publishing Group.

Peng T, Thorn K, Schroeder T, Wang L, Theis FJ, Marr C, and Navab N (2017) A BaSiC tool for background and shading correction of optical microscopy images. *Nat Commun* **8**:14836–7, Nature Publishing Group.

Pickford P, Lucey M, Fang Z, Bitsi S, la Serna de JB, Broichhagen J, Hodson DJ, Minnion J, Rutter GA, Bloom SR, Tomas A, and Jones B (2020) Signalling, trafficking and glucoregulatory properties of glucagon-like peptide-1 receptor agonists exendin-4 and lixisenatide. *Br J Pharmacol* bph.15134, John Wiley & Sons, Ltd.

Roed SN, Nøhr AC, Wismann P, Iversen H, Bräuner-Osborne H, Knudsen SM, and Waldhoer M (2015) Functional consequences of glucagon-like peptide-1 receptor cross-talk and trafficking. *J Biol Chem* **290**:1233–1243, American Society for Biochemistry and Molecular Biology.

Roed SN, Wismann P, Underwood CR, Kulahin N, Iversen H, Cappelen KA, Schäffer L, Lehtonen J, Hecksher-Soerensen J, Secher A, Mathiesen JM, Bräuner-Osborne H, Whistler JL, Knudsen SM, and Waldhoer M (2014) Real-time trafficking and signaling of the glucagon-like peptide-1 receptor. *Mol Cell Endocrinol* **382**:938–949.

Sage D, Donati L, Soulez F, Fortun D, Schmit G, Seitz A, Guiet R, Vonesch C, and Unser M (2017) DeconvolutionLab2: An open-source software for deconvolution microscopy. *Methods* **115**:28–41.

Surdo NC, Berrera M, Koschinski A, Brescia M, Machado MR, Carr C, Wright P, Gorelik J, Morotti S, Grandi E, Bers DM, Pantano S, and Zaccolo M (2017) FRET biosensor uncovers cAMP nano-domains at β-adrenergic targets that dictate precise tuning of cardiac contractility. *Nat Commun* **8**:15031.

Thornton K, and Gorenstein DG (1994) Structure of glucagon-like peptide (7-36) amide in a dodecylphosphocholine micelle as determined by 2D NMR. *Biochemistry* **33**:3532–3539.

Tiulpakov A, White CW, Abhayawardana RS, See HB, Chan AS, Seeber RM, Heng JI, Dedov I, Pavlos NJ, and Pfleger KDG (2016) Mutations of Vasopressin Receptor 2 Including Novel L312S Have Differential Effects on Trafficking. *Mol Endocrinol* **30**:889–904.

Tomas A, Jones B, and Leech C (2019) New Insights into Beta-Cell GLP-1 Receptor and cAMP Signaling. *J Mol Biol*, doi: 10.1016/j.jmb.2019.08.009.

Trier S, Linderoth L, Bjerregaard S, Andresen TL, and Rahbek UL (2014) Acylation of Glucagon-like peptide-2: interaction with lipid membranes and in vitro intestinal permeability. *PLoS ONE* **9**:e109939, Public Library of Science.

van der Westhuizen ET, Breton B, Christopoulos A, and Bouvier M (2014) Quantification of ligand bias for clinically relevant β2-adrenergic receptor ligands: implications for drug taxonomy. *Mol Pharmacol* **85**:492–509.

Vilardaga J-P, Jean-Alphonse FG, and Gardella TJ (2014) Endosomal generation of cAMP in GPCR signaling. *Nat Chem Biol* **10**:700–706.

Villar VAM, Cuevas S, Zheng X, and Jose PA (2016) Localization and signaling of GPCRs in lipid rafts. *Methods Cell Biol* **132**:3–23, Elsevier.

Downloaded from molpharm.aspetjournals.org at ASPET Journals on April 20, 2024

Wan Q, Okashah N, Inoue A, Nehmé R, Carpenter B, Tate CG, and Lambert NA (2018) Mini G protein probes for active G protein-coupled receptors (GPCRs) in live cells. *J Biol Chem* **293**:7466–7473.

Widmann C, Dolci W, and Thorens B (1995) Agonist-induced internalization and recycling of the glucagon-like peptide-1 receptor in transfected fibroblasts and in insulinomas. *Biochem J* **310 (Pt 1)**:203–214.

Willard FS, Douros JD, Gabe MB, Showalter AD, Wainscott DB, Suter TM, Capozzi ME, van der Velden WJ, Stutsman C, Cardona GR, Urva S, Emmerson PJ, Holst JJ, D'Alessio DA, Coghlan MP, Rosenkilde MM, Campbell JE, and Sloop KW (2020) Tirzepatide is an imbalanced and biased dual GIP and GLP-1 receptor agonist. *JCI Insight* **5**:1202.

Wu F, Yang L, Hang K, Laursen M, Wu L, Han GW, Ren Q, Roed NK, Lin G, Hanson MA, Jiang H, Wang M-W, Reedtz-Runge S, Song G, and Stevens RC (2020) Full-length human GLP-1 receptor structure without orthosteric ligands. *Nat Commun* **11**:1272.

Zhang H, Sturchler E, Zhu J, Nieto A, Cistrone PA, Xie J, He L, Yea K, Jones T, Turn R, Di Stefano PS, Griffin PR, Dawson PE, McDonald PH, and Lerner RA (2015) Autocrine selection of a GLP-1R G-protein biased agonist with potent antidiabetic effects. *Nat Commun* **6**:8918–13, Nature Publishing Group.

Zhang J, Bai Q, Pérez-Sánchez H, Shang S, An X, and Yao X (2019) Investigation of ECD conformational transition mechanism of GLP-1R by molecular dynamics simulations and Markov state model. *Phys Chem Chem Phys* **21**:8470–8481.

Zhao P, Liang Y-L, Belousoff MJ, Deganutti G, Fletcher MM, Willard FS, Bell MG, Christe ME, Sloop KW, Inoue A, Truong TT, Clydesdale L, Furness SGB, Christopoulos A, Wang M-W, Miller LJ, Reynolds CA, Danev R, Sexton PM, and Wootten D (2020) Activation of the GLP-1 receptor by a non-peptidic agonist. *Nature* **577**:432–436.

Ziomkiewicz I, Loman A, Klement R, Fritsch C, Klymchenko AS, Bunt G, Jovin TM, and Arndt-Jovin DJ (2013) Dynamic conformational transitions of the EGF receptor in living mammalian cells determined by FRET and fluorescence lifetime imaging microscopy. *Cytometry A* **83**:794–805.

Downloaded from molpharm.aspetjournals.org at ASPET Journals on April 20, 2024

Molecular Pharmacology Fast Forward. Published on July 27, 2021 as DOI: 10.1124/molpharm.121.000270
This article has not been copyedited and formatted. The final version may differ from this version.

Footnotes:

The Section of Endocrinology and Investigative Medicine is funded by grants from the Medical Research Council, Biotechnology and Biological Sciences Research Council National Institute of Health Research (NIHR) and is supported by the NIHR Biomedical Research Centre Funding Scheme. The views expressed are those of the authors and not necessarily those of the funders. This project was also supported by the Medical Research Council (MR/R010676/1, MR/N00275X/1 and MR/S025618/1, and MR/N020081/1), the Imperial Post-doctoral Post-CCT Research Fellowship scheme, the European Federation for the Study of Diabetes, Diabetes UK (including grant 17/0005681), the Academy of Medical Sciences, Society for Endocrinology, The British Society for Neuroendocrinology, the Engineering and Physical Sciences Research Council, the European Research Council under the European Union's Horizon 2020 research and innovation programme (Starting Grant 715884), UKRI Future Leaders Fellowship (MR/S031537/1), Fondation de la Recherche Médicale (Equipe FRM DEQ20130326503, EQU201903008055), Agence Nationale de la Recherche (ANR-19-CE16-0025-01, ANR-15-CE14-0025-02), Institut National de la Santé et de la Recherche Médicale (INSERM), and Centre National de la Recherche Scientifique (CNRS).

BioRxiv Footnote. "An earlier version of this paper appears in bioRxiv under the doi BIORXIV/2021/438030

Financial disclosure: none

Downloaded from molpharm.aspetjournals.org at ASPET Journals on April 20, 2024

Molecular Pharmacology Fast Forward. Published on July 27, 2021 as DOI: 10.1124/molpharm.121.000270
This article has not been copyedited and formatted. The final version may differ from this version.

Main Figure Legends

Figure 1. Biased agonism with exendin-4 and exendin-4-C16. (**A**) Schematic depicting the amino acid sequences of exendin-4 and exendin-4-C16 in single letter amino acid code. (**B**) Equilibrium binding of unmodified exendin-4 and exendin-4-C16, *n*=5, measured by competition binding in HEK293-SNAP-GLP1-R cells with exendin(9-39)-FITC used as the competing probe. (**C**) cAMP response in HEK293-SNAP-GLP-1R cells, 30 min stimulation, *n*=5, with 4-parameter fits shown after normalisation to global maximum. (**D**) LgBiT-mini-G_s (mG_s) and LgBit-β-arrestin-2 (βarr2) recruitment to GLP-1R-SmBiT, *n*=5, with 3-parameter concentration-responses constructed from AUCs, and bias factor calculation (see methods) with comparison by paired t-test. (**E**) Measurement of $G\alpha_s$ activation in HEK293T cells transiently transfected with SNAP-GLP-1R-NLuc and Nb37-GFP and stimulated with 100 nM agonist or vehicle, *n*=6, with AUCs compared by paired t-test. Refer to Supplementary Figure 5B for individual experimental repeats. (**F**) Measurement of β-arrestin-2 activation in HEK293T cells transiently transfected with SNAP-GLP-1R and NLuc-4myc-βarr2-CYOFP1 and stimulated with 100 nM agonist or vehicle, *n*=5, with AUCs compared by paired t-test. (**G**) Heatmap representation of 100 nM agonist response data shown in Figure 1B-F with normalisation to exendin-4 response. (**H**) Insulin secretion in INS-1 832/3 cells stimulated for 60 min with each agonist at 11 mM glucose (G11), *n*=4, paired t-test. (**I**) As for (H) but 16 h stimulation, *n*=6. Data are shown as mean ± SEM with individual replicates shown in some cases. * $p<0.05$ by statistical test indicated.

Figure 2. Visualisation of GLP-1R endocytosis with exendin-4 and exendin-4-C16, and fluorescent agonist conjugates. (**A**) Representative images from *n*=3 experiments demonstrating endocytosis of SNAP-GLP-1R labelled with SNAP-Surface-549 after treatment for 30 min with 100 nM agonist or vehicle; scale bars = 8 µm. (**B**) Time-lapse images demonstrating movement of surface-labelled SNAP-GLP-1R into punctate structures on stimulation with 100 nM agonist or vehicle; scale bars = 20 µm. The graphs show the

Downloaded from molpharm.aspetjournals.org at ASPET Journals on April 20, 2024

Molecular Pharmacology Fast Forward. Published on July 27, 2021 as DOI: 10.1124/molpharm.121.000270
This article has not been copyedited and formatted. The final version may differ from this version.

change over time in "spot count" per 0.33 mm field-of-view (FOV) after normalisation to cell confluence, with the concentration-dependent rate constant (K) derived from one-phase association fitting also plotted with a 3-parameter fit. (**C**) Representative images showing endosomal uptake of exendin-4 and exendin-4-TMR in T-REx-SNAP-GLP-1R cells with or without tetracycline-induced GLP-1R expression, labelled with SNAP-Surface-649 prior to stimulation with 100 nM of each TMR-conjugate for 30 min. Scale bars = 8 µm. Data are shown as mean ± SEM.

Figure 3. Subcellular targeting of exendin-4 and exendin-4-C16. (**A**) Schematic depicting the investigation of GLP-1R membrane trafficking using the TR-FRET and BRET assays used in this work. (**B**) GLP-1R disappearance from cell surface in HEK293-SNAP-GLP-1R cells treated with 100 nM agonist or vehicle, measured by DERET, *n*=5. (**C**) GLP-1R translocation to late endosomes / lysosomes in HEK293-SNAP-GLP-1R cells treated with 100 nM agonist or vehicle, measured by TR-FRET using Lysotracker Red DND99 as the acceptor, *n*=5. (**D**) GLP-1R recycling in HEK293-SNAP-GLP-1R cells previously treated for 30 min with 100 nM agonist, measured by TR-FRET using extracellular Luxendin645 as the acceptor, *n*=5. (**E**) Heatmap representation of data shown in (B), (C) and (D) after normalisation to the exendin-4 response; statistical significance is indicated after paired t-test. (**F**) GLP-1R disappearance from the cell surface in HEK293T cells transiently transfected with SNAP-GLP-1R-NLuc and KRAS-venus and treated with 100 nM agonist or vehicle, measured by BRET, *n*=6. (**G**) GLP-1R appearance in Rab5+ early endosomes in HEK293T cells transiently transfected with SNAP-GLP-1R-NLuc and KRAS-venus and treated with 100 nM agonist or vehicle, measured by BRET, *n*=6. (**H**) As for (G) but for Rab7+ late endosomes, *n*=7. (**I**) As for (G) but for Rab11+ recycling endosomes, *n*=7. (**J**) Heatmap representation of data shown in (F), (G), (H) and (I) after normalisation to the exendin-4 response; statistical significance is indicated from paired t-tests. (**K**) Mini-G_s translocation to the plasma membrane or Rab5+ early endosomes in HEK293-SNAP-GLP-1R cells treated with 100 nM agonist after transient transfection with Mini-G_s-NLuc plus

Downloaded from molpharm.aspetjournals.org at ASPET Journals on April 20, 2024

Molecular Pharmacology Fast Forward. Published on July 27, 2021 as DOI: 10.1124/molpharm.121.000270
This article has not been copyedited and formatted. The final version may differ from this version.

KRAS-venus or Rab5-venus, *n*=5. The agonist-specific AUC measured for each compartment marker are ratiometrically compared by paired t-test. Data are shown as mean ± SEM with individual replicates shown in some cases. * p<0.05 by statistical test indicated.

Figure 4. Membrane interactions of C-terminally acylated exendin-4 conjugates. (**A**) Confocal microscopy and phase contrast images of GUVs incubated with exendin-4-FITC or exendin-4-FITC-C16. Scale bars = 5 µm. Membrane signal is represented on the line plot. (**B**) FRET spectrum from T-REx-SNAP-GLP-1R cells with or without tetracycline-induced GLP-1R expression, labelled with 50 nM NR12S and incubated with 100 nM exendin-4-FITC or exendin-4-FITC-C16, *n*=7. The background spectrum of each FITC ligand was subtracted and the trace was normalised to the signal at 525 nm. Peak emission wavelength and amplitude, derived from Gaussian fitting of each spectrum, are shown and compared between ligands by 2-way randomised block ANOVA with Sidak's test. (**C**) FRET imaging of T-REx-SNAP-GLP-1R cells stimulated with 1 µM exendin-4 or exendin-4-C16, with representative ratiometric images pre- and post-stimulation, and quantification from *n*=3 experiments. (**D**) Matched comparison of nanodomain-specific cAMP (AKAP79-CUTie) and total cAMP (HTRF) in T-REx-SNAP-GLP-1R cells, 12 min stimulation, *n*=6, with ΔpEC_{50} comparison by paired t-test. (**E**) cAMP responses in HEK293-SNAP-GLP-1R cells pre-incubated for 30 min with vehicle or 10 mM MβCD, prior to stimulation with each ligand for 30 min. Responses are expressed relative to the forskolin (FSK; 10 µM) response, *n*=5, with the effect of MβCD on potency shown by subtracting pEC_{50} results and comparison by paired t-test. (**F**) GLP-1R internalisation measured by DERET in HEK293-SNAP-GLP-1R cells pre-incubated for 30 min with vehicle or 10 mM MβCD prior to stimulation with each ligand at 100 nM for 30 min, *n*=5. AUC relative to baseline was quantified and +MβCD results expressed relative to -MβCD results for each ligand, and compared by paired t-test. (**G**) Principle of NR12S conformational biosensor assay, with kinetic responses showing TR-FRET ratio normalised to baseline in response to indicated concentration of exendin-4 or exendin-4-C16, *n*=5, with concentration response curve constructed from AUC with 3-

Downloaded from molpharm.aspetjournals.org at ASPET Journals on April 20, 2024

Molecular Pharmacology Fast Forward. Published on July 27, 2021 as DOI: 10.1124/molpharm.121.000270
This article has not been copyedited and formatted. The final version may differ from this version.

parameter fit. Data are shown as mean ± SEM with individual replicates where possible. * $p<0.05$ by statistical test indicated.

Figure 5. Albumin binding by fluorescence correlation spectroscopy and *in vivo* effects. (**A**) Diffusion coefficients, D ($\mu m^2 s^{-1}$), of indicated concentration of indicated ligand with and without 0.1% BSA, with comparison by 2-way randomised block ANOVA with Sidak's test. (**B**) Representative 1x 3D free diffusion fit for Exendin4-TMR-C16 (20 nM) autocorrelation curves with or without 0.1% BSA. The autocorrelation function, G(τ), is normalised to facilitate comparison of decay curves. (**C**) Molecular brightness, ε (counts per molecule per second), of EX4-TMR-C16 (20 nM) with and without 0.1% BSA. (**D**) Cumulative food intake in male HFD mice (n=8/group) after a single IP injection of the indicated agonist. Statistical comparisons between equimolar agonist doses by 2-way repeated measures ANOVA with Tukey's test. (**E**) As for (B) but showing the effect on body weight. (**F**) IPGTT (2g/kg glucose) performed at the start and end of the 72-hour study. AUCs are compared by 1-way ANOVA with Sidak's test for equimolar agonist doses. Data are shown as mean ± SEM with individual replicates shown in some cases. * $p<0.05$ by statistical test indicated.

Downloaded from molpharm.aspetjournals.org at ASPET Journals on April 20, 2024

Molecular Pharmacology Fast Forward. Published on July 27, 2021 as DOI: 10.1124/molpharm.121.000270
This article has not been copyedited and formatted. The final version may differ from this version.

Table 1. Pharmacological parameters of exendin-4 and exendin-4-C16. Mean ± SEM parameter estimates from concentration-response analyses in Figure 1. * p<0.05 by paired t-test.

	Exendin-4	**Exendin-4-C16**
Binding affinity (HEK293-SNAP-GLP-1R, *n*=5)		
Log K_i (M)	-9.2 ± 0.1	-8.8 ± 0.1 *
Cyclic AMP (HEK293-SNAP-GLP-1R, *n*=5)		
Log EC_{50} (M)	-9.7 ± 0.1	-9.5 ± 0.1
E_{max} (% global max)	101 ± 2	98 ± 3
Hill slope	2.1 ± 0.3	1.8 ± 0.3
Mini-G_s recruitment (HEK293T, *n*=5)		
Log EC_{50} (M)	-8.2 ± 0.1	-8.3 ± 0.1
E_{max}	268 ± 23	171 ± 14 *
β-arrestin-2 recruitment (HEK293T, *n*=5)		
Log EC_{50} (M)	-7.6 ± 0.1	-7.7 ± 0.1
E_{max} (AUC)	66 ± 16	25 ± 5 *
Insulin secretion (INS-1 832/3, *n*=6)		
Log EC_{50} (M)	-11.0 ± 0.2	-10.6 ± 0.1 *
E_{max}	1.7 ± 0.1	2.2 ± 0.2*

Downloaded from molpharm.aspetjournals.org at ASPET Journals on April 20, 2024

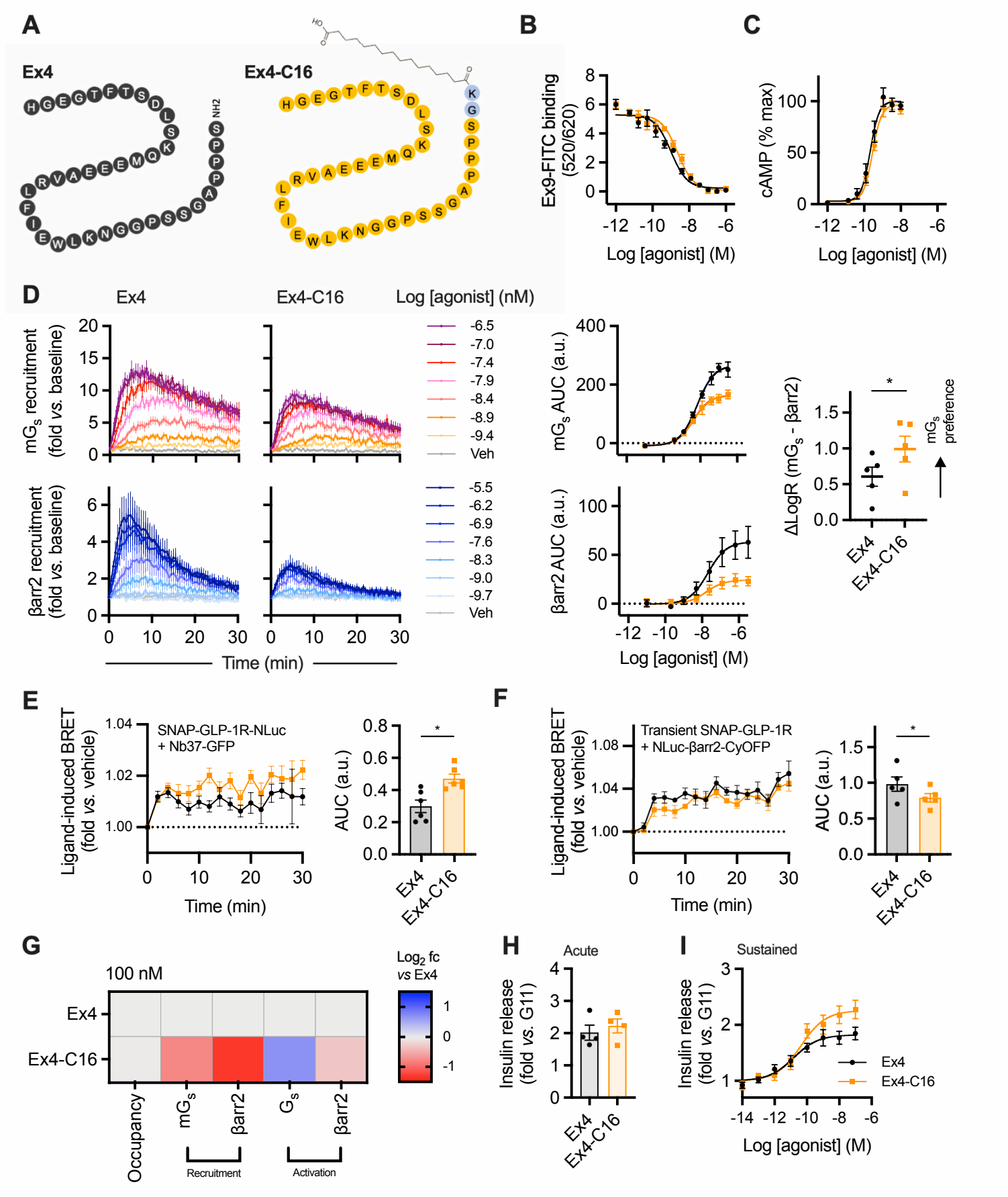
A
Ex4
Ex4-C16
NH2
B
Ex9-FITC binding (520/620)
Log [agonist] (M)
C
cAMP (% max)
Log [agonist] (M)
D
Ex4
Ex4-C16
Log [agonist] (nM)
mGs recruitment (fold vs. baseline)
βarr2 recruitment (fold vs. baseline)
-6.5
-7.0
-7.4
-7.9
-8.4
-8.9
-9.4
Veh
-5.5
-6.2
-6.9
-7.6
-8.3
-9.0
-9.7
Veh
Time (min)
mGs AUC (a.u.)
βarr2 AUC (a.u.)
Log [agonist] (M)
ΔLogR (mGs - βarr2)
mGs preference
Ex4
Ex4-C16
E
SNAP-GLP-1R-NLuc + Nb37-GFP
Ligand-induced BRET (fold vs. vehicle)
Time (min)
AUC (a.u.)
Ex4
Ex4-C16
F
Transient SNAP-GLP-1R + NLuc-βarr2-CyOFP
Ligand-induced BRET (fold vs. vehicle)
Time (min)
AUC (a.u.)
Ex4
Ex4-C16
G
100 nM
Ex4
Ex4-C16
Occupancy
mGs
βarr2
Gs
βarr2
Recruitment
Activation
Log2 fc vs Ex4
H
Acute
Insulin release (fold vs. G11)
Ex4
Ex4-C16
I
Sustained
Insulin release (fold vs. G11)
Ex4
Ex4-C16
Log [agonist] (M)

Figure 1

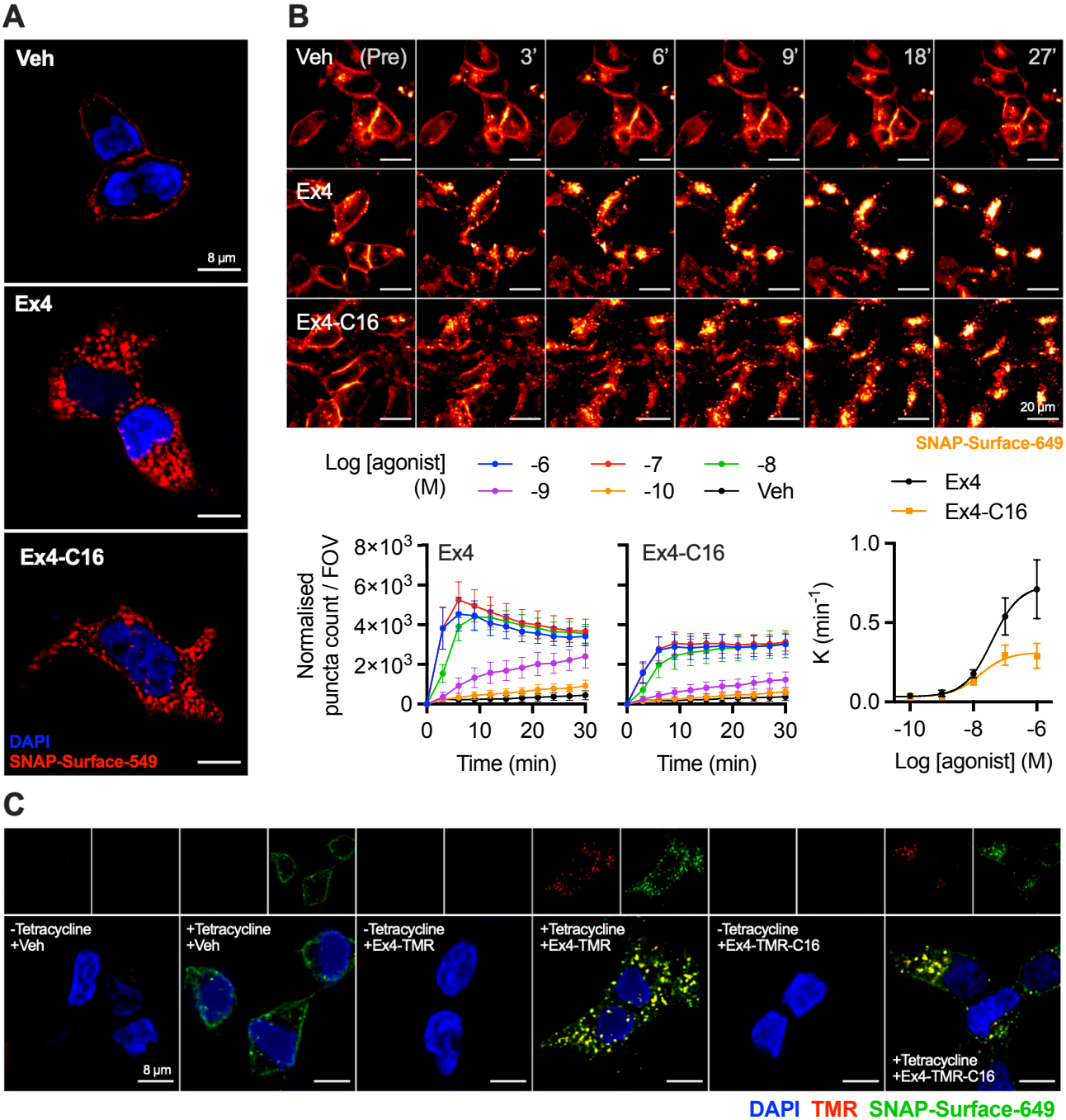
A
Veh
8 µm
Ex4
Ex4-C16
DAPI
SNAP-Surface-549
B
Veh (Pre)
3'
6'
9'
18'
27'
Ex4
Ex4-C16
20 µm
SNAP-Surface-649
Log [agonist] (M)
-6
-7
-8
-9
-10
Veh
Ex4
Ex4-C16
Normalised puncta count / FOV
8×10^3
6×10^3
4×10^3
2×10^3
0
Time (min)
K (min^-1)
1.0
0.5
0.0
-10
-8
-6
Log [agonist] (M)
C
-Tetracycline +Veh
+Tetracycline +Veh
-Tetracycline +Ex4-TMR
+Tetracycline +Ex4-TMR
-Tetracycline +Ex4-TMR-C16
+Tetracycline +Ex4-TMR-C16
8 µm
DAPI TMR SNAP-Surface-649

Figure 2

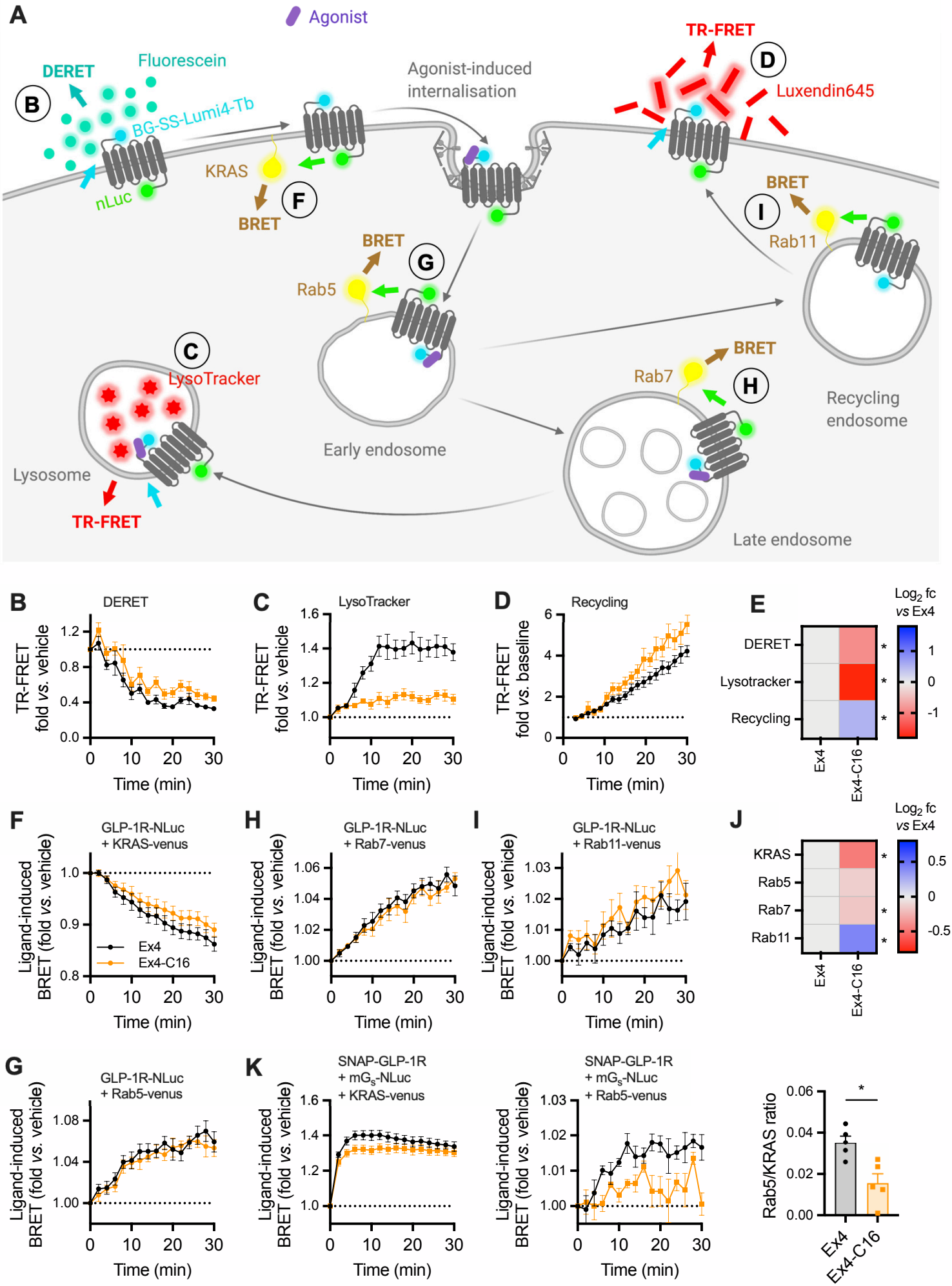
A
Agonist
DERET
Fluorescein
B
BG-SS-Lumi4-Tb
nLuc
KRAS
BRET
F
Agonist-induced
internalisation
TR-FRET
D
Luxendin645
BRET
I
Rab11
BRET
G
Rab5
C
LysoTracker
Lysosome
TR-FRET
Early endosome
BRET
Rab7
H
Recycling
endosome
Late endosome
B
DERET
TR-FRET
fold vs. vehicle
Time (min)
C
LysoTracker
TR-FRET
fold vs. vehicle
Time (min)
D
Recycling
TR-FRET
fold vs. baseline
Time (min)
E
Log2 fc
vs Ex4
DERET
Lysotracker
Recycling
Ex4
Ex4-C16
F
GLP-1R-NLuc
+ KRAS-venus
Ligand-induced
BRET (fold vs. vehicle)
Ex4
Ex4-C16
Time (min)
H
GLP-1R-NLuc
+ Rab7-venus
Ligand-induced
BRET (fold vs. vehicle)
Time (min)
I
GLP-1R-NLuc
+ Rab11-venus
Ligand-induced
BRET (fold vs. vehicle)
Time (min)
J
Log2 fc
vs Ex4
KRAS
Rab5
Rab7
Rab11
Ex4
Ex4-C16
G
GLP-1R-NLuc
+ Rab5-venus
Ligand-induced
BRET (fold vs. vehicle)
Time (min)
K
SNAP-GLP-1R
+ mGs-NLuc
+ KRAS-venus
Ligand-induced
BRET (fold vs. vehicle)
Time (min)
SNAP-GLP-1R
+ mGs-NLuc
+ Rab5-venus
Ligand-induced
BRET (fold vs. vehicle)
Time (min)
Rab5/KRAS ratio
Ex4
Ex4-C16

Figure 3

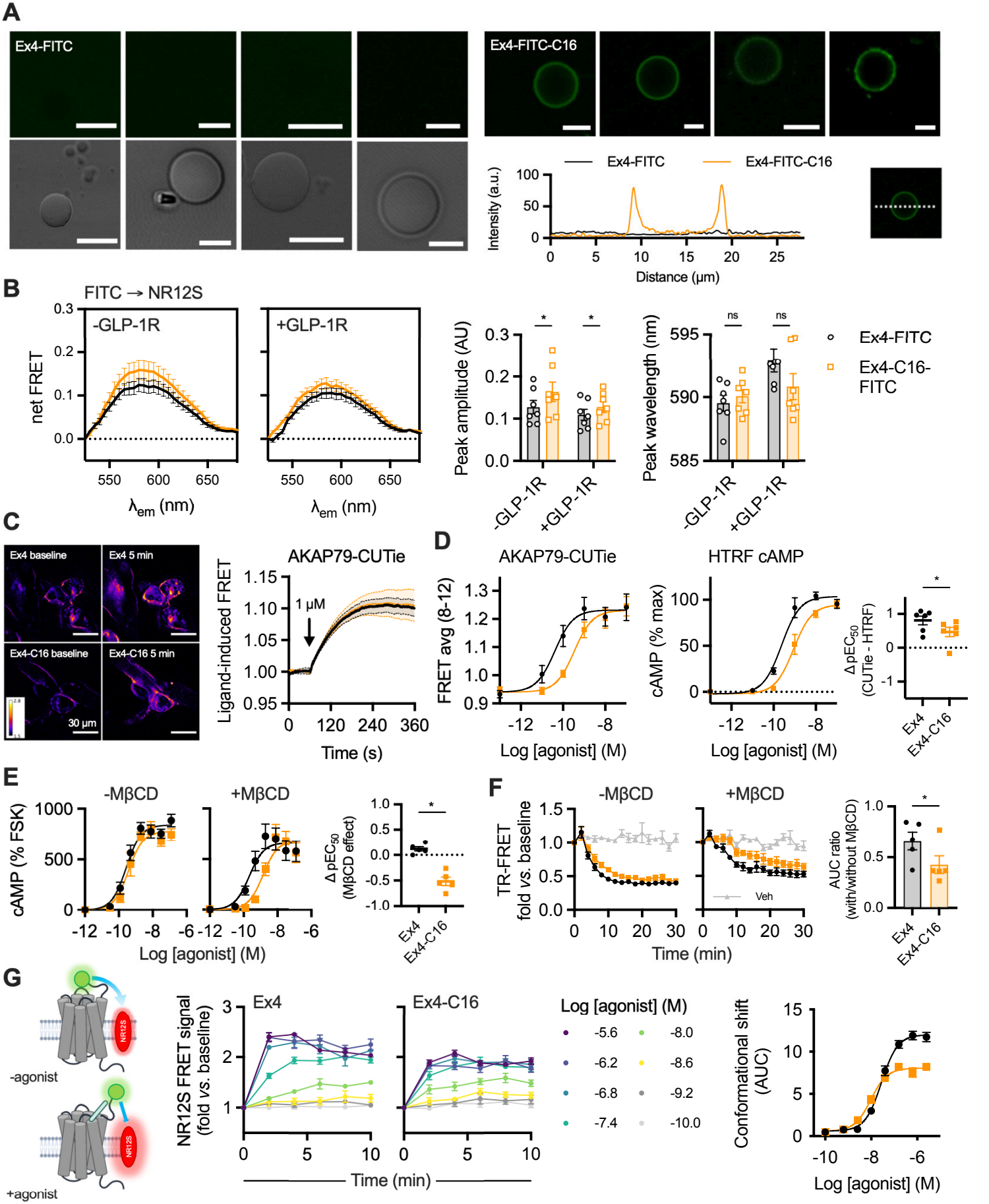
A
Ex4-FITC
Ex4-FITC-C16
Intensity (a.u.)
Distance (µm)
B
FITC → NR12S
-GLP-1R
+GLP-1R
net FRET
λem (nm)
Peak amplitude (AU)
Peak wavelength (nm)
ns
Ex4-FITC
Ex4-C16-FITC
C
Ex4 baseline
Ex4 5 min
Ex4-C16 baseline
Ex4-C16 5 min
30 µm
AKAP79-CUTie
Ligand-induced FRET
1 µM
Time (s)
D
AKAP79-CUTie
HTRF cAMP
FRET avg (8-12)
cAMP (% max)
Log [agonist] (M)
ΔpEC50 (CUTie - HTRF)
Ex4
Ex4-C16
E
-MβCD
+MβCD
cAMP (% FSK)
Log [agonist] (M)
ΔpEC50 (MβCD effect)
F
TR-FRET fold vs. baseline
Veh
Time (min)
AUC ratio (with/without MβCD)
G
NR12S
-agonist
+agonist
NR12S FRET signal (fold vs. baseline)
Log [agonist] (M)
-5.6
-6.2
-6.8
-7.4
-8.0
-8.6
-9.2
-10.0
Conformational shift (AUC)

Figure 4

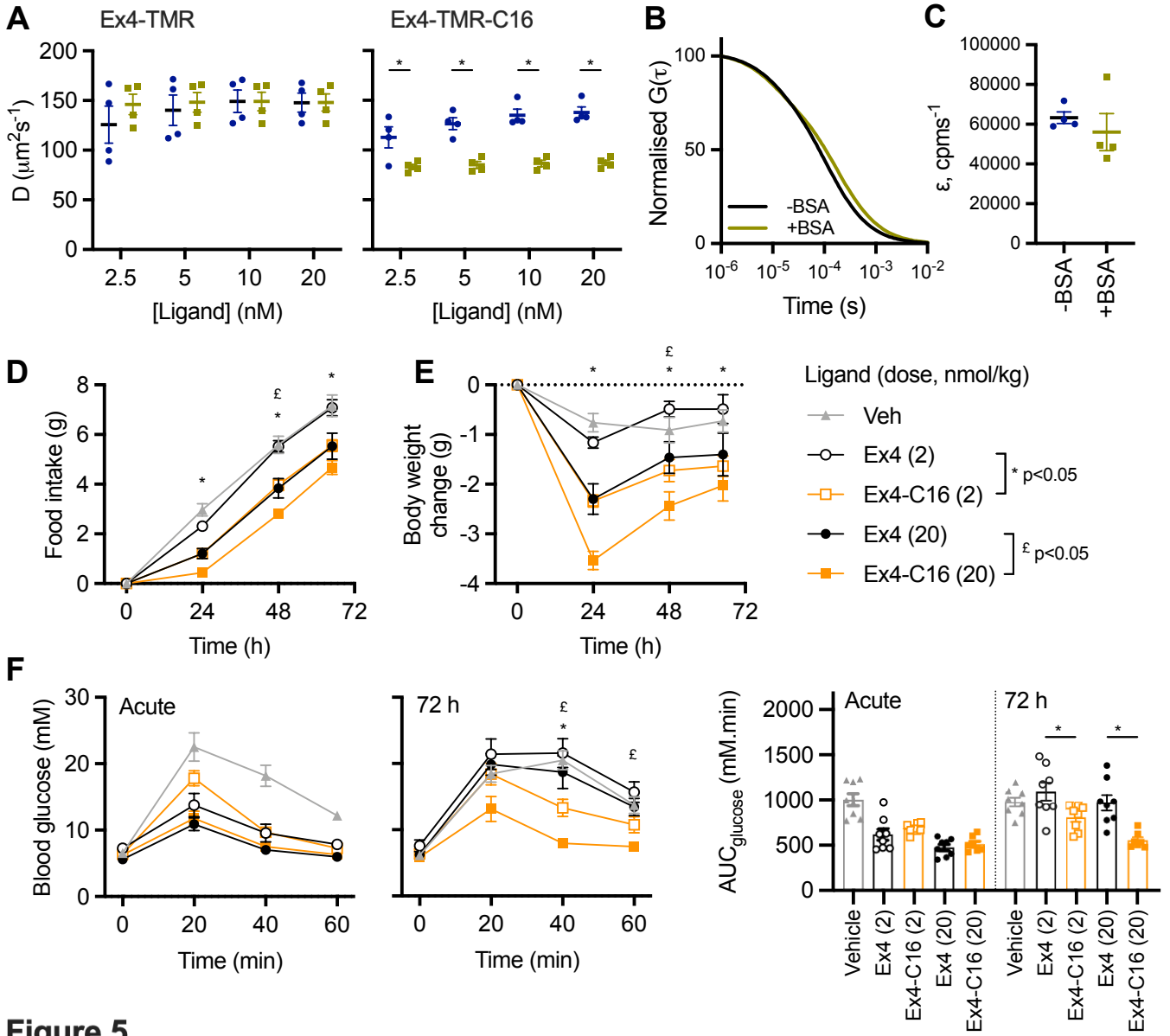
A
Ex4-TMR
Ex4-TMR-C16
D (μm²s⁻¹)
[Ligand] (nM)
B
Normalised G(τ)
-BSA
+BSA
Time (s)
C
ε, cpms⁻¹
-BSA
+BSA
D
Food intake (g)
Time (h)
E
Body weight change (g)
Time (h)
Ligand (dose, nmol/kg)
Veh
Ex4 (2)
Ex4-C16 (2)
Ex4 (20)
Ex4-C16 (20)
* p<0.05
£ p<0.05
F
Acute
72 h
Blood glucose (mM)
Time (min)
AUCglucose (mM.min)
Vehicle
Ex4 (2)
Ex4-C16 (2)
Ex4 (20)
Ex4-C16 (20)

Figure 5